Cell

ATP Synthase c-Subunit Leak Causes Aberrant Cellular Metabolism in Fragile X Syndrome

Graphical Abstract

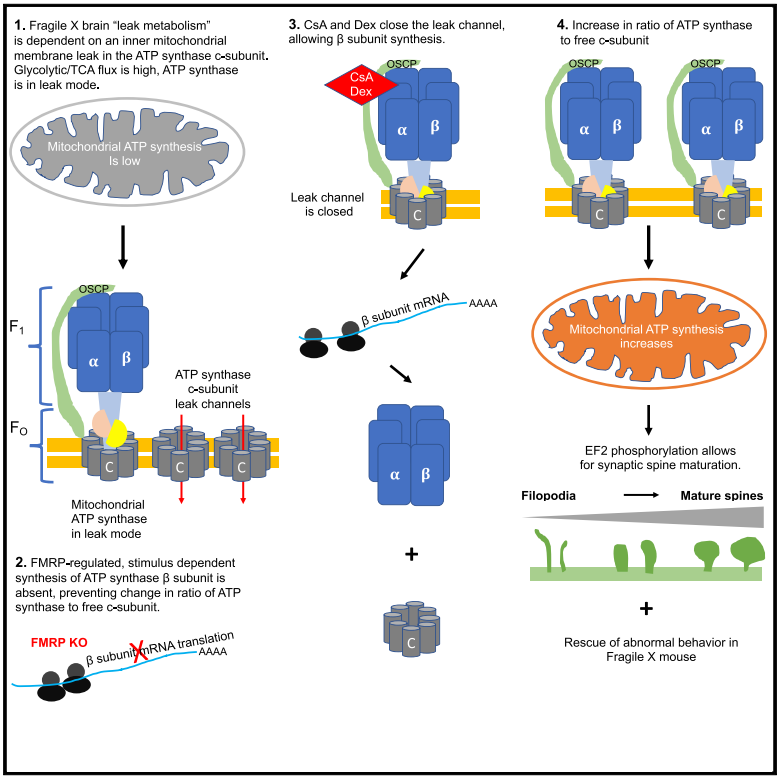

Highlights

- ATP synthase c-subunit leak in Fragile X causes aberrant metabolism
- Changes in ATP synthase component stoichiometry regulate protein synthesis rate
- Inhibition of the leak normalizes synaptic spine morphology and Fragile X behavior

Authors

Pawel Licznerski, Han-A Park, Harshvardhan Rolyan, ..., Valentin K. Gribkoff, Richard J. Levy, Elizabeth A. Jonas

Correspondence

pawel.licznerski@yale.edu (P.L.), elizabeth.jonas@yale.edu (E.A.J.)

In Brief

Lack of FMRP in Fragile X neurons is associated with a leak in the ATP synthase, the blockade of which normalizes cellular and behavioral disease phenotypes.

Licznerski et al., 2020, Cell *182*, 1–16
September 3, 2020
https://doi.org/10.1016/j.cell.2020.07.008

Please cite this article in press as: Licznerski et al., ATP Synthase c-Subunit Leak Causes Aberrant Cellular Metabolism in Fragile X Syndrome, Cell (2020), https://doi.org/10.1016/j.cell.2020.07.008

Cell

CellPress

Article

ATP Synthase c-Subunit Leak Causes Aberrant Cellular Metabolism in Fragile X Syndrome

Pawel Licznerski,[1,*] Han-A Park,[1,5] Harshvardhan Rolyan,[1] Rongmin Chen,[1] Nelli Mnatsakanyan,[1] Paige Miranda,[1] Morven Graham,[2] Jing Wu,[1] Nicole Cruz-Reyes,[4] Nikita Mehta,[4] Sana Sohail,[4] Jorge Salcedo,[4] Erin Song,[4] Charles Effman,[4] Samuel Effman,[4] Lucas Brandao,[6] Gulan N. Xu,[1] Amber Braker,[1] Valentin K. Gribkoff,[1,4] Richard J. Levy,[3] and Elizabeth A. Jonas[1,4,7,*]

[1]Department of Internal Medicine, Section of Endocrinology, Yale University School of Medicine, New Haven, CT 06511, USA
[2]Department of Cell Biology, Yale University School of Medicine, New Haven, CT 06520, USA
[3]Department of Anesthesiology, Columbia University Medical Center, New York, NY 10032, USA
[4]Marine Biological Laboratory, Woods Hole, MA 02543, USA
[5]Department of Human Nutrition and Hospitality Management, College of Human Environmental Sciences, The University of Alabama, Tuscaloosa, AL 35487, USA
[6]Department of Biology, Clark University, Worcester, MA 01610, USA
[7]Lead Contact
*Correspondence: pawel.licznerski@yale.edu (P.L.), elizabeth.jonas@yale.edu (E.A.J.)
https://doi.org/10.1016/j.cell.2020.07.008

SUMMARY

Loss of the gene (*Fmr1*) encoding Fragile X mental retardation protein (FMRP) causes increased mRNA translation and aberrant synaptic development. We find neurons of the *Fmr1*$^{-/y}$ mouse have a mitochondrial inner membrane leak contributing to a "leak metabolism." In human Fragile X syndrome (FXS) fibroblasts and in *Fmr1*$^{-/y}$ mouse neurons, closure of the ATP synthase leak channel by mild depletion of its c-subunit or pharmacological inhibition normalizes stimulus-induced and constitutive mRNA translation rate, decreases lactate and key glycolytic and tricarboxylic acid (TCA) cycle enzyme levels, and triggers synapse maturation. FMRP regulates leak closure in wild-type (WT), but not FX synapses, by stimulus-dependent ATP synthase β subunit translation; this increases the ratio of ATP synthase enzyme to its c-subunit, enhancing ATP production efficiency and synaptic growth. In contrast, in FXS, inability to close developmental c-subunit leak prevents stimulus-dependent synaptic maturation. Therefore, ATP synthase c-subunit leak closure encourages development and attenuates autistic behaviors.

INTRODUCTION

Fragile X syndrome (FXS) is a devastating X-linked genetic disorder and the most common inherited cause of intellectual disability (Dölen et al., 2010; Wijetunge et al., 2013). It results from a CGG repeat expansion within the *Fmr1* gene that leads to loss of expression of Fragile X mental retardation protein (FMRP). The FX phenotype is characterized by constitutively increased mRNA translation rates, morphological immaturity of synapses and dendritic spines (Dölen et al., 2007), aberrant synaptic plasticity (Bear et al., 2004), excitotoxicity (Dölen et al., 2007, 2010), and enhanced excitability (Brown et al., 2010; Deng et al., 2013; El-Hassar et al., 2019; McCullagh et al., 2020; Strumbos et al., 2010; Zhang et al., 2012). The structural and functional deficiencies in FX neurons correlate with loss of normal learning patterns and an increase in autistic behaviors (Santos et al., 2014) in rodents and humans (Zoghbi and Bear, 2012). Despite the fact that FMRP has been well described as an RNA-binding protein (Darnell, 2011; Darnell et al., 2011), there have been, to date, no effective therapies for the disorder.

Prior work found that depletion of *Fmr1* and its homolog *Fxr2* reduces fat deposits in mutant mice and leads to higher food intake, increased oxygen consumption, and CO_2 production, suggesting uncoupled oxidative phosphorylation (Lumaban and Nelson, 2015). In human autism spectrum disorder patients, elevated lactate levels, indicative of glycolysis driven by mitochondrial dysfunction, have been described (Dhillon et al., 2011; Goh et al., 2014). Hippocampal neurons of the *Fmr1* CGG repeat knockin (KI) mouse (FMRP levels decreased by 42.6%) have small mitochondria with reduced mobility, high O_2 uptake, and a large proton leak (Kaplan et al., 2012). In a recent report, *Drosophila fmr1* was found to alter the metabolome of the flies such that the *dfmr1* mutants had decreased carbohydrate and lipid stores, were hypersensitive to starvation stress, hyperphagic, and had reduced NAD^+/NADH ratio (Weisz et al., 2018). This was related to a defect in mitochondria producing an increase in maximal respiratory capacity. A recent report also found that, in *Fmr1*$^{-/y}$ mouse brains, electron transport complexes run at high rates even though ATP production is low, suggesting inner membrane inefficiency (H^+ ion leak) (D'Antoni et al.,

Please cite this article in press as: Licznerski et al., ATP Synthase c-Subunit Leak Causes Aberrant Cellular Metabolism in Fragile X Syndrome, Cell (2020), https://doi.org/10.1016/j.cell.2020.07.008

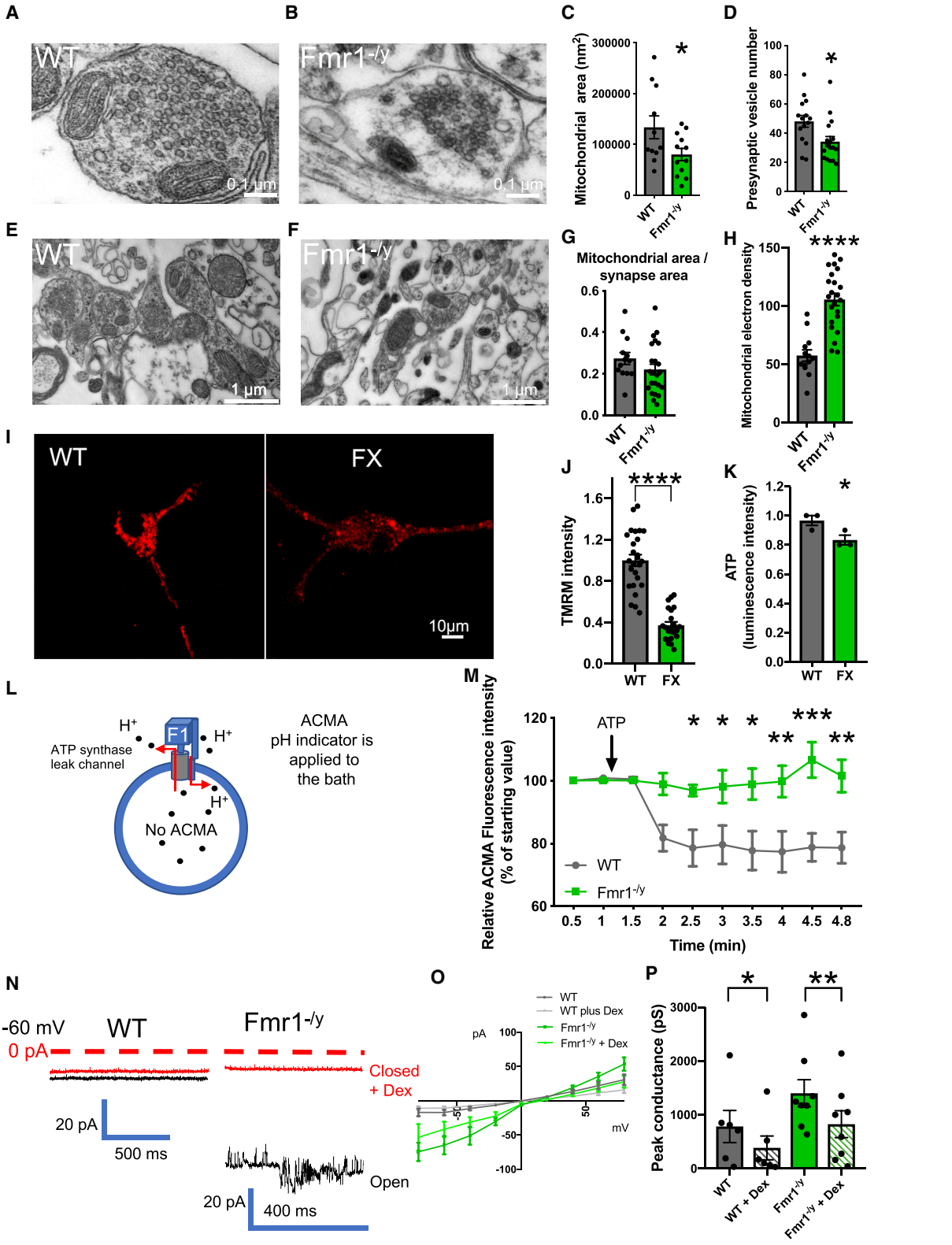

Figure 1. *Fmr1*$^{-/y}$ Mitochondria Have an Inner Mitochondrial Membrane Leak

(A and B) Representative electron microscopy images of brain slices show smaller synapses within the CA1 region of the mouse *Fmr1*$^{-/y}$ hippocampus compared to WT.

(legend continued on next page)

Please cite this article in press as: Licznerski et al., ATP Synthase c-Subunit Leak Causes Aberrant Cellular Metabolism in Fragile X Syndrome, Cell (2020), https://doi.org/10.1016/j.cell.2020.07.008

2020). Our group's recent report shows that mitochondria from the *Fmr1*$^{-/y}$ mouse brains have inefficient thermogenic respiration due to a futile coenzyme Q-regulated proton leak, leading to synaptic spine and behavioral abnormalities (Griffiths et al., 2020). Although these findings suggest that FMRP and related proteins might be required in general for normal developmental mitochondrial function, they also highlight the possibility that FX mitochondria are uncoupled and have an inner membrane leak that makes the mitochondria inefficient, burning fuel instead of saving energy.

The mitochondrial abnormalities could be emblematic of neuronal immaturity. Several findings indicate that FX neurons are underdeveloped (Bassell and Warren, 2008; Bhattacharya et al., 2012; Pyronneau et al., 2017). They have redundant postsynaptic spines with a thin, long filopodial shape that has failed to change to a mushroom shape characteristic of mature synapses (Bagni and Greenough, 2005). FX mitochondria are also small (Kaplan et al., 2012). The possibility that this structural immaturity throughout brain development is related to the delay of a metabolic shift during development is suggested by reports on cardiac development in the early wild-type (WT) embryo. At embryonic day (E) 9.5 profound inner mitochondrial membrane leak accompanies a lack of respiration (Hom et al., 2011). The leak closes between E11.5 and E13.5 at the onset of oxidative phosphorylation (Hom et al., 2011) and respiration becomes coupled to phosphorylation. This normal developmental process is related to closure of the cell death channel that spans the mitochondrial inner membrane, known as the permeability transition pore (mPTP), and development is hastened by the mPTP inhibitor cyclosporine A (CsA) (Beutner et al., 2014, 2017).

We have reported previously that certain proteins and pharmacological reagents regulate directly mitochondrial inner membrane efficiency by binding to the ATP synthase enzymatic (F_1) portion (Alavian et al., 2011, 2015; Chen et al., 2011, 2019). Our work indicates that a leak that regulates inner membrane ATP production efficiency resides within the membrane-embedded c-subunit ring of the ATP synthase (Alavian et al., 2014). We have further suggested that the c-subunit ring may form or contribute significantly to the CsA regulated mPTP (Alavian et al., 2014; Bernardi and Di Lisa, 2015; Bonora et al., 2013; Mnatsakanyan et al., 2019; Neginskaya et al., 2019; Rasola and Bernardi, 2014). We have shown recently that the mPTP is aberrantly active in *Fmr1*$^{-/y}$ mitochondria (Griffiths et al., 2020).

We now suggest that the mitochondrial inner membrane leak of FX neurons and cells is caused by abnormally high levels of ATP synthase c-subunit. We find that the c-subunit leak causes persistence of an immature metabolic phenotype associated specifically with mitochondrial leak, termed here "leak metabolism." The c-subunit leak aberrantly elevates protein synthesis; a decrease in c-subunit level or specific pharmacological inhibition of ATP synthase leak reduces protein synthesis rates and decreases the leak metabolism in the neurons. In keeping with the c-subunit leak as causative of abnormally delayed neuronal development, we find that inhibition of the ATP synthase leak allows for the maturation of synapses and normalizes autistic behaviors in a mouse model of FX.

RESULTS

Mitochondrial Morphology and Function Are Altered in FX Mouse Neurons

Mitochondria are necessary for normal synapse formation and thus mitochondria themselves undergo developmental plasticity; large changes in mitochondrial structure and function occur during development (Brandt et al., 2017; McCarron et al., 2013). We therefore examined mitochondria in *Fmr1*$^{-/y}$ neurons and compared them to mitochondria of WT neurons of the same age. Electron micrographs taken of hippocampal CA1 brain slices prepared from 2-month-old mice revealed that presynaptic vesicle pools were smaller in *Fmr1*$^{-/y}$ synapses than those of WT synapses as previously described (Figures 1A, 1B, and 1D) (Klemmer et al., 2011). The mitochondria within *Fmr1*$^{-/y}$ synapses also had a decreased area compared to WT synapses (Figures 1A–1C), but the ratio of mitochondrial area to synapse area was similar in *Fmr1*$^{-/y}$ versus WT synapses (Figures 1E–1G), suggesting that mitochondrial size was scaled to

(C) Group data show a decrease in mitochondrial area in *Fmr1*$^{-/y}$ compared to WT (-n = 15 for *Fmr1*$^{-/y}$ and –n = 17 micrographs for WT, *p = 0.043).
(D) The vesicle number in presynaptic boutons is reduced in *Fmr1*$^{-/y}$ (n= 11 micrographs of each condition; *p = 0.0143).
(E and F) Example electron micrographs of synapses from the CA1 region of the mouse hippocampus slices show that *Fmr1*$^{-/y}$ synapses contain electron dense mitochondria not present in WT synapses.
(G) Mitochondrial area/synapse area is unchanged comparing WT to *Fmr1*$^{-/y}$ (n = 13 micrographs for WT and 23 for *Fmr1*$^{-/y}$).
(H) Group data show electron density is increased in *Fmr1*$^{-/y}$ compared to WT (n= 23 micrographs for *Fmr1*$^{-/y}$ and 13 for WT; *p = 0.0114).
(I) Representative images of mitochondrial membrane potential indicator TMRM fluorescence in isolated cortical neurons.
(J) Group data show TMRM intensity is reduced in FX compared to WT (n= 20–24 neurons each condition, 4 independent cultures; ****p < 0.0001).
(K) Cytosolic ATP levels of isolated cortical neurons are reduced in FX compared to WT (n = 3 wells for each, *p < 0.05).
(L) Illustration of method of measurement of bath H^+ ion concentration using the H^+ sensitive indicator ACMA. SMVs are illustrated with mitochondrial ATP synthase F_1 facing toward the bath. ATP hydrolysis causes H^+ ion sequestration into the lumen of the vesicles. Vesicles are impermeant to the pH indicator. Red arrows show paths of H^+ pumping (at the side of the c-subunit) and H^+ leak (through the center of the c-subunit).
(M) Lack of sequestration of H^+ ions into *Fmr1*$^{-/y}$ SMVs during ATP hydrolysis by the ATP synthase (n = 3 samples per condition).
(N) Representative patch clamp recordings of SMVs of *Fmr1*$^{-/y}$ and WT at the indicated holding potential. Black trace indicates open channel. Red trace shows the relatively closed channel in the same recording after Dex exposure.
(O) Current voltage relationship for the group of SMV recordings shown in (P).
(P) Group data of peak conductances of the independent recordings (n= 6 for WT and WT+Dex; n = 8 for *Fmr1*$^{-/y}$ and *Fmr1*$^{-/y}$ +Dex) measured from 0 pA (*p = 0.0449 comparing WT to WT+Dex; **p = 0.0064 comparing *Fmr1*$^{-/y}$ to *Fmr1*$^{-/y}$+Dex). Linear current voltage relationship was assumed for calculation of peak conductance. In (C), (D), (G), (H), (J), and (K), unpaired two-tailed Student's t test was used. In (M), two-way repeated-measures ANOVA followed by Sidak's multiple comparison test was used. In (P), paired two-way Student's t test was used. Data are represented as mean ± SEM (*p < 0.05; **p < 0.01; ***p < 0.001; ****p < 0.0001).

Please cite this article in press as: Licznerski et al., ATP Synthase c-Subunit Leak Causes Aberrant Cellular Metabolism in Fragile X Syndrome, Cell (2020), https://doi.org/10.1016/j.cell.2020.07.008

the smaller synaptic size in *Fmr1*$^{-/y}$. The mitochondria of *Fmr1*$^{-/y}$ synapses had no apparent disturbance of cristae structure, although there was a marked increase in matrix density relative to that of controls (Figures 1E, 1F, and 1H), possibly reflecting a high protein amount within the matrix compartment.

To examine mitochondrial function at an earlier stage of development, we prepared cortical neurons from mice at postnatal days (P) 1–2 and studied them at the time when synapses are forming rapidly (DIV14). Mitochondrial inner membrane polarization is indicative of appropriate use of the electron transport chain. Using the membrane potential indicator tetramethylrhodamine methyl ester (TMRM), we determined that FX mitochondria generated less than half the membrane potential of the mitochondria of WT neurons (Figures 1I and 1J). Lack of membrane potential can arise from rapid ATP production caused by inability to keep up with increased energy demand or from depolarization caused by a mitochondrial inner membrane leak. In either case, ATP levels may be decreased. In fact, ATP levels in FX neurons were slightly decreased compared to WT control neurons (Figure 1K), suggesting that FX neurons fall behind in their combined mitochondrial and glycolytic ATP production.

Fmr1$^{-/y}$ Mitochondria Have a Large Conductance Inner Membrane Leak

In the setting of increased energy demand, H^+ ions move across the mitochondrial ATP synthase and cause a conformational change in the ATP synthase molecular complex that results in ATP production. The enzyme can also hydrolyze ATP to provide energy to translocate H^+ ions across the inner mitochondrial membrane in reverse mode. The 9-amino-6-chloro-2-methoxyacridine (ACMA) assay measures the ATP synthase enzymatic rate using this reverse mode (Figure 1L) (Caviston et al., 1998). To perform this assay, mitochondrial inner membrane remnants that are relatively enriched in ATP synthase (submitochondrial vesicles [SMVs]) are prepared (Chan et al., 1970; Chen et al., 2004; Ko et al., 2003). In these SMVs, the F_1 or enzymatic portion of the ATP synthase is exposed to the medium, which contains a membrane impermeant H^+ indicator. SMVs prepared from WT brain readily sequestered H^+ ions in response to the addition of ATP to the bath. In contrast, *Fmr1*$^{-/y}$ SMVs failed to sequester H^+ ions in response to ATP addition (Figure 1M), indicating either failure of the enzyme to translocate H^+ or an H^+ leak in the SMV membranes. To detect directly an inner mitochondrial membrane leak, we analyzed patch clamp recordings of *Fmr1*$^{-/y}$ brain SMVs. We found a large multi-conductance, voltage-dependent channel activity not present in WT brain SMVs (Figures 1N–1P), indicating that lack of sequestration of H^+ ions in the ACMA assay was due to loss of the H^+ ions through an open channel in the SMV membranes.

Our previous reports demonstrated an effect of an ATP synthase modulator, dexpramipexole (Dex) on inner mitochondrial membrane leak channel activity (Alavian et al., 2015). It had been described previously that Dex, which is the R(+) enantiomer of the widely used Parkinson's drug, Pramipexole, has no significant dopaminergic efficacy, is not a CsA analog, and it readily crosses the blood brain barrier (Bozik et al., 2010; Cudkowicz et al., 2011). We reported that radiolabeled Dex binds to ATP synthase F_O subunit b and F_1 subunit oligomycin sensitivity conferring protein (OSCP), closing an inner membrane leak in patch clamp recordings, enhancing ATP production efficiency and decreasing cell death and oxygen consumption with modest potency (Alavian et al., 2015). To test if ATP synthase leak was the cause of the open channel in *Fmr1*$^{-/y}$ SMVs, we applied Dex during the recordings. Dex decreased small conductance activity of the WT SMVs and decreased large conductance channel activity in the *Fmr1*$^{-/y}$ SMVs as measured by change in peak conductance (Figured 1N and 1P). This suggests that at least some of the leak in *Fmr1*$^{-/y}$ mitochondrial inner membranes is produced by increased activity of the ATP synthase leak channel, although a resistant fraction of the leak could be produced by uncomplexed c-subunit or by other channels.

ATP synthase contains a highly regulated, multi-conductance channel that is contained within the c-subunit ring of the main membrane bound (F_O) portion (Alavian et al., 2014; Mnatsakanyan et al., 2019). Pathological opening of the channel may occur upon conformational change of the ATP synthase including loss of an inhibitory structure in its cavity (Gerle, 2016; Gu et al., 2019; Mnatsakanyan and Jonas, 2020; Vlasov et al., 2019), separation of the F_1 from the F_O (Alavian et al., 2014), or loss of F_1 (Chen et al., 2019). We hypothesized, based on these previous findings and the channel recording data, that the ratio of c-subunit (F_O) to F_1 might be altered such that *Fmr1*$^{-/y}$ mitochondria could have an unopposed (uncoupled to F_1) c-subunit that would readily leak ions across the inner mitochondrial membrane in a voltage-dependent manner. We found, in *Fmr1*$^{-/y}$, that ATP synthase β-subunit (a major part of the soluble enzyme or F_1 component) level was markedly elevated above that measured in control mitochondria (Figure 2A), but the level of c-subunit (F_O) was elevated to an even greater degree (Figure 2A). To determine if this resulted in free c-subunit in the mitochondrial membrane, we subjected mitochondrial proteins to non-denaturing Native-PAGE electrophoresis (Figure 2B). These immunoblots showed that, although total amounts of assembled ATP synthase monomer plus dimer were not significantly elevated in *Fmr1*$^{-/y}$ compared to WT, level of free c subunit was markedly elevated compared to WT controls. We analyzed the blots in two ways. In the same blot, we compared the level of *Fmr1*$^{-/y}$ fully assembled ATP synthase (monomer plus dimer) to the WT controls and the level of *Fmr1*$^{-/y}$ free c-subunit to the WT controls (left set of histograms). In the right histogram, we calculated the ratio of free c-subunit to its own assembled ATP synthase within the same lane. Both analyses showed that free c-subunit is markedly elevated in *Fmr1*$^{-/y}$ compared to WT controls.

We next carried out experiments to determine if the increase in β and c subunit levels in *Fmr1*$^{-/y}$ mitochondria can be attributed directly to FMRP-regulated mRNA translation. Many of the nuclear-encoded mRNAs for components of the ATP synthase have been found to bind FMRP in crosslinking immunoprecipitation experiments, and mRNA for the ATP synthase β subunit is the 87th most represented on the list of over 800 mRNAs (Darnell et al., 2011). To confirm the binding of FMRP to ATP synthase β-subunit mRNA, we immunoprecipitated FMRP from synaptoneurosomal (hereafter synaptosomal) lysates and performed PCR on the cDNA synthesized from the immunoprecipitate. We confirmed that FMRP binds β subunit mRNA. By reverse transcription PCR (RT-PCR), ATP5G2 was found to be by far

Please cite this article in press as: Licznerski et al., ATP Synthase c-Subunit Leak Causes Aberrant Cellular Metabolism in Fragile X Syndrome, Cell (2020), https://doi.org/10.1016/j.cell.2020.07.008

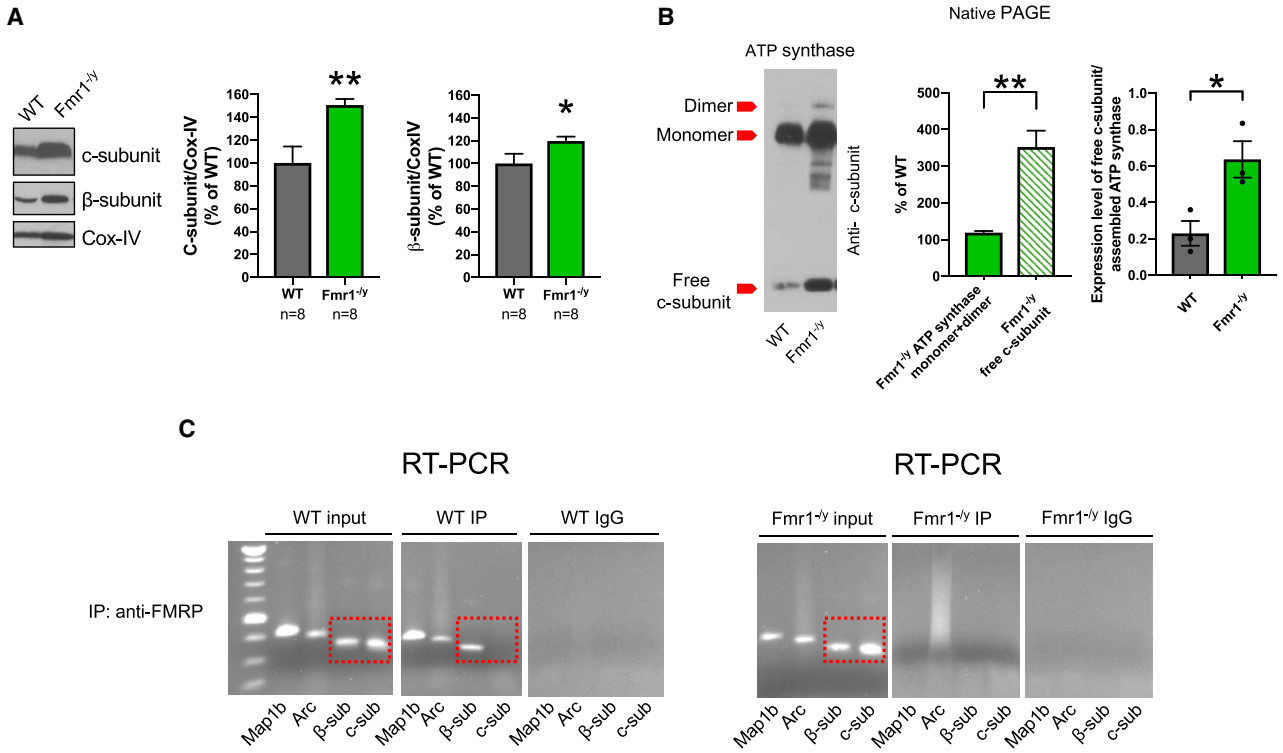

Figure 2. Expression of ATP Synthase Subunits Causing Inner Membrane Leak Is Increased in *Fmr1*$^{-/y}$ Mitochondria

(A) c- and β-subunit protein expression levels are higher in *Fmr1*$^{-/y}$ brain mitochondria compared to those of WT (n = 8 independent samples for each, **p = 0.0083 and *p = 0.031).

(B) An example of three independent experiments of non-denaturing Native-PAGE electrophoresis of isolated brain mitochondria. Immunoblotting performed with anti-c-subunit antibody. The abundance of the free c-subunit is higher in *Fmr1*$^{-/y}$ mitochondria compared to WT. Left histograms: level of fully assembled ATP synthase (monomer plus dimer) and the level of free c-subunit in *Fmr1*$^{-/y}$ as a percent of WT control. Right histograms: ratio of free c-subunit to its own assembled ATP synthase within the same lane. n = 3 for each condition.

(C) FMRP immunoprecipitation from isolated synaptosomes pulls down ATP synthase β-subunit mRNA but not ATP synthase c-subunit mRNA (ATP5G2) as detected by RT-PCR (shown is one of n= 3 independent immunoprecipitation experiments). All experiments in this figure used unpaired Student's t test, data are represented as mean ± SEM (*p < 0.05; **p < 0.01; ***p < 0.001; ****p < 0.0001).

See also Figure S1 and Table S2.

the dominant c-subunit gene, but we failed to detect binding of FMRP to any of the three c-subunit gene products (only ATP5G2 is shown in Figure 2C). In *Fmr1*$^{-/y}$ synapses, quantitative real-time PCR (qRT-PCR) of the synaptosomes (Figure S1), performed to detect total expression of ATP synthase β subunit and ATP5G2 c-subunit mRNA, showed that these mRNAs were elevated compared to those of WT synapses. Therefore, although loss of FMRP may lead to enhanced transcription of both ATP synthase β and c-subunit mRNAs, in contrast only β subunit, but not c-subunit, translation is likely to be regulated by FMRP. Taken together, these results suggest a role for FMRP in ATP synthase assembly during activity-dependent synaptic development (see Figure 5D).

FX Neurons Have a Mitochondrial Leak-Dependent Metabolic Phenotype

Despite the leaky inner membrane, ATP levels were only slightly decreased in FX neurons compared to controls (Figure 1K), suggesting that glycolytic ATP might contribute to the overall ATP level in the neuronal cytoplasm. To determine the metabolic phenotype of the neurons, we labeled newly synthesized proteins with puromycin and immunoprecipitated with an anti-puromycin antibody. We then evaluated the newly synthesized proteome by liquid chromatography with tandem mass spectrometry (LC-MS/MS) (Figures 3A and 3B; Table S1). This study revealed that FX neurons have an increase in certain glycolytic enzymes including hexokinase II, pyruvate kinase M2 variant and lactate dehydrogenase, and also in enzymes required for tricarboxylic acid (TCA) cycle and NAD^+/NADH metabolism, including enzymes of the malate/aspartate shunt and isocitrate dehydrogenase (Dayton et al., 2016; Li et al., 2016; Roberts and Miyamoto, 2015; Vander Heiden et al., 2009; Zheng et al., 2016). Because these data suggested an increase in activity of glycolytic enzymes, we measured lactate levels and found that they were markedly increased in the FX culture media (Figure 3 C). High glycolytic activity and lactate production, but also increases in TCA cycle enzymes, are hallmark features of immature and developing cells (Fame et al., 2019). Although puromycin incorporation into newly translating proteins provided us with an estimate of the high translation rate of metabolic enzymes, it did not

Please cite this article in press as: Licznerski et al., ATP Synthase c-Subunit Leak Causes Aberrant Cellular Metabolism in Fragile X Syndrome, Cell (2020), https://doi.org/10.1016/j.cell.2020.07.008

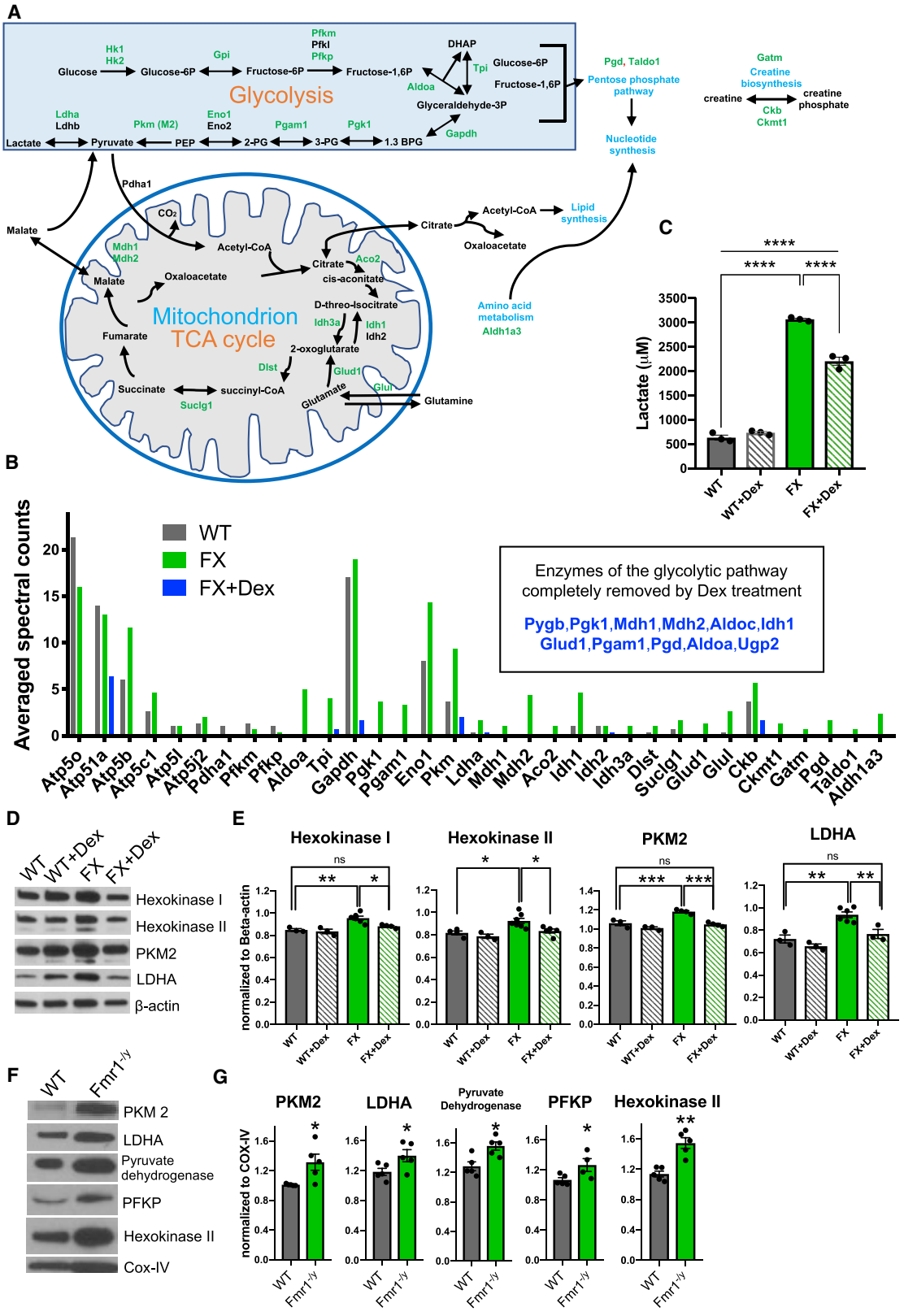

(legend on next page)

Please cite this article in press as: Licznerski et al., ATP Synthase c-Subunit Leak Causes Aberrant Cellular Metabolism in Fragile X Syndrome, Cell (2020), https://doi.org/10.1016/j.cell.2020.07.008

tell us about the steady state levels of these enzymes. To test if specific enzymes are elevated in FX, we performed immunoblots on WT and FX neuronal cultures and brain mitochondria. These showed that the levels of certain key enzymes are elevated in FX (Figures 3D–3G), including hexokinase and pyruvate dehydrogenase, suggestive not only of enhanced glycolytic flux but also of enhanced TCA cycle function, supporting the idea that increased flux through the FX mitochondria is caused by the mitochondrial inner membrane leak. Because Dex closed the mitochondrial inner membrane leak in patch clamp recordings, and we reported previously that Dex enhances the efficiency of oxidative phosphorylation (Alavian et al., 2015), we tested if Dex treatment of the FX neuronal cultures would eliminate the increased flux of the leak metabolic phenotype. We found that Dex effectively decreased the lactate levels in FX neurons; it also reversed the abnormally high levels of glycolytic and TCA enzymes (Figures 3B–3D). These results are consistent with increased flux through glycolytic and TCA pathways caused by the inner membrane leak in FX. Dex normalizes the aberrant leak metabolism of FX neurons through its actions to close the ATP synthase leak.

Genetic or Pharmacological Modulation of ATP Synthase Leak Decreases Abnormally Elevated Protein Synthesis Rates in FX

Previous work has shown that the anti-apoptotic protein Bcl-xL acts on the ATP synthase to close the mitochondrial inner membrane leak (Alavian et al., 2011; Chen et al., 2011), but whether this is tied to changes in protein synthesis rate was not known. Both translation of the reporter Dendra (Figures S2A and S2B), and puromycin incorporation assays (Figures 4E–4H) demonstrated that rates of mRNA translation in general are elevated in FX neurons compared to WT, as has been described previously (Bear et al., 2004; Dölen et al., 2007; Jacquemont et al., 2018; Muscas et al., 2019; Udagawa et al., 2013). We found that rates of Dendra translation or puromycin incorporation were similarly elevated in WT neurons by exposure to the selective Bcl-xL inhibitor ABT-737 (Figures S2C–S2E), and in contrast, these rates were reduced by Bcl-xL protein transfection into synapses (Figures S2F and S2G). These findings are consistent with the hypothesis that opening of the ATP synthase leak (Alavian et al., 2011) increases overall mRNA translation rates in developing neurons. The pertinent pharmacological reagents (Dex and CsA) and Bcl-xL all bind in the soluble portion (F_1) of the ATP synthase, not within the membrane embedded portion. Therefore, to determine if membrane-embedded ATP synthase c-subunit leak channel directly modulates mRNA translation rate, we depleted c-subunit protein by small interfering RNA (siRNA) or increased c-subunit protein level by overexpression in human FX fibroblasts and measured protein synthesis rates by puromycin incorporation. We found that mild depletion of c-subunit decreased protein synthesis rate (Figure 4A) and, in contrast, c-subunit overexpression increased the rate of protein synthesis (Figure 4B), directly implicating c-subunit leak in regulation of protein synthesis rate in human FX cells. In FX cortical neurons, the ATP synthase leak inhibitor Dex also decreased protein synthesis rates in a concentration-dependent manner (Figures 4C and 4D), consistent with Dex effects on decreasing the open probability of the ATP synthase leak channel. Application of Dex also decreased protein synthesis in brain slices (Figures 4E and 4F). We then tested a well-known and more potent inhibitor of the ion channel conductance of the ATP synthase that also inhibits the mPTP, CsA (Baines et al., 2005; Nakagawa et al., 2005). CsA prevents binding of cyclophilin D to ATP synthase subunit OSCP (Giorgio et al., 2009, 2013). In FX neuronal cultures, small concentrations of CsA readily reversed the aberrantly increased mRNA translation rate (Figures 4G and 4H), but had no effect on mRNA translation in WT neurons (Figures 4G and 4H), suggesting that the CsA-sensitive leak is larger in FX compared to WT neuronal mitochondria (see Figures 1N–1P).

We also carried out electron microscopy to visualize the effects of CsA on the protein synthetic machinery in the CA1 region of hippocampal slices from *Fmr1*$^{-/y}$ and WT mice. Slices were treated with CsA or vehicle for 2.5 h then fixed for processing. Our studies showed a large increase in the number of actively translating ribosomal assemblies (rosettes) in *Fmr1*$^{-/y}$ CA1 neurons, consistent with an enhancement in mRNA translation over that seen in WT neurons (Figures 4I–4N). Strikingly, CsA greatly reduced the number of rosettes in the contralateral half of the same coronal brain slice, suggesting that its effects on mitochondrial inner membrane leak rapidly decreased the rate of mRNA translation in *Fmr1*$^{-/y}$ CA1 neurons.

Figure 3. Metabolic Profile of FX Cortical Neurons Shows Enhancement of Glycolysis/TCA Flux in FX Compared to WT

(A) Glycolysis and tricarboxylic acid (TCA) cycle schematics illustrating enzymes involved in both pathways. Enzymes increased in FX > WT in at least 2 of 3 independent cultures are labeled in green.

(B) Averaged spectral counts of metabolic peptides expressed in WT and FX cortical neuron cultures. Puromycin immunoprecipitates were analyzed by LC-MS/MS after cortical neuronal cultures (DIV14) were exposed to puromycin for 15 min. Shown in blue are the enzymes decreased by Dex treatment in at least 2 out of 3 FX cultures (n = 3 independent cultures of each condition). Metabolic peptides completely removed by Dex treatment are indicated above the graph in blue lettering.

(C) Lactate levels are elevated in the culture media collected from FX primary neurons compared to those of WT. Exposure of FX neurons to Dex significantly decreases lactate levels in the media.

(D) Representative immunoblots of WT and FX cortical cultures exposed to vehicle or Dex.

(E) Quantification of blots shown in (D). At least 3 independent cultures were used. A set of 4 key enzymes is elevated in FX compared to WT. Dex treatment normalizes the protein levels of all enzymes in the set.

(F) Representative immunoblots of WT and *Fmr1*$^{-/y}$ mitochondria isolated from brain.

(G) Quantification of blots shown in (F). At least three animals per condition. Glycolytic enzymes and pyruvate dehydrogenase protein levels are elevated in *Fmr1*$^{-/y}$ mitochondrial fractions. In (C) and (E), two-way ANOVA followed by Tukey's multiple comparisons test was used. In (G), unpaired two-tailed Student's t test was used. Data are represented as mean ± SEM (*$p < 0.05$; **$p < 0.01$; ***$p < 0.001$; ****$p < 0.0001$).

See also Table S1.

Please cite this article in press as: Licznerski et al., ATP Synthase c-Subunit Leak Causes Aberrant Cellular Metabolism in Fragile X Syndrome, Cell (2020), https://doi.org/10.1016/j.cell.2020.07.008

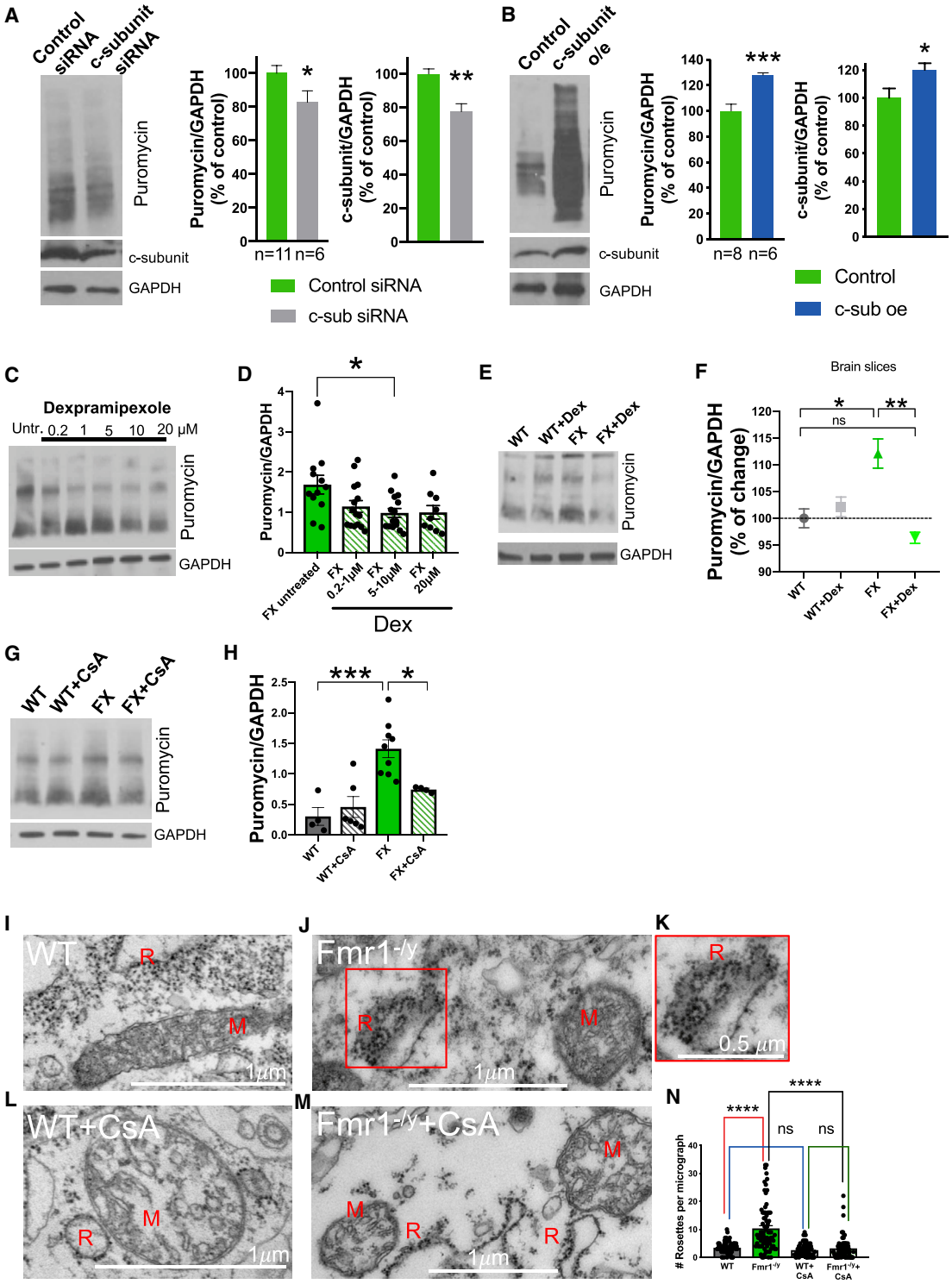

Figure 4. Inhibition of the Mitochondrial Inner Membrane Leak Decreases Protein Synthesis in FX

(A) c-subunit depletion in human FX fibroblasts decreases the rate of protein synthesis. Representative puromycin (top), c-subunit immunoblots (middle), and protein controls (bottom) are shown at left. Quantification of the immunoblots is shown at right.

(B) c-subunit overexpression in human FX fibroblasts increases the rate of protein synthesis. Representative blots of puromycin and c-subunit are shown at left as in (A). Quantification of the immunoblots is shown at right.

(legend continued on next page)

Please cite this article in press as: Licznerski et al., ATP Synthase c-Subunit Leak Causes Aberrant Cellular Metabolism in Fragile X Syndrome, Cell (2020), https://doi.org/10.1016/j.cell.2020.07.008

Abnormally Enhanced Mitochondrial Inner Membrane Leak Prevents Stimulus-Dependent Protein Synthesis

FX neuronal synapses have abnormal stimulus-dependent synaptic plasticity and ineffective synapse maturation (Pfeiffer and Huber, 2009; Sidorov et al., 2013). We considered that inefficient ATP production by mitochondria in FX synapses could compromise stimulation-dependent phosphorylation events of the protein synthesis machinery, thereby affecting synaptic growth. The translation of mRNAs for synaptic proteins during long term changes in synaptic plasticity is regulated by an increase in phosphorylation of elongation factor 2 (EF2) ~5 min after neuronal stimulation (Autry and Monteggia, 2012; Gildish et al., 2012; Park et al., 2008; Scheetz et al., 2000; Um et al., 2013). We found that stimulation of WT synaptosomes using the NMDA glutamate receptor co-agonist D-serine led to robust phosphorylation of EF2 at 5 min followed by increased protein synthesis at 30 min, as has been reported previously (Figures 5A–5C) (Scheetz et al., 2000). Strikingly, both EF2 phosphorylation and protein synthesis changes failed to occur following synaptic stimulation in *Fmr1*$^{-/y}$ synapses (Figures 5A–5C). If the mitochondrial membrane leak were responsible for the failure of phosphorylation of EF2 during synaptic stimulation, then this specific phosphorylation event would be rescued by closing the leak. Indeed, application of low dose CsA completely rescued EF2 phosphorylation and restored the normal pattern of protein synthesis upon synaptic stimulation in *Fmr1*$^{-/y}$ synapses (Figures 5A–5C), confirming that this phosphorylation event and subsequent changes in protein synthesis rate are sensitive to ATP synthase leak modulation.

One potential mechanism by which FMRP could regulate the leak across the inner mitochondrial membrane is by controlling the translation of FMRP-bound mRNA coding for the ATP synthase β subunit. A stimulus-induced increase in protein levels of β subunit would decrease the level of free c-subunit by assembling the full F_1F_O ATP synthase. To test this, we measured β subunit protein levels in the same stimulated synaptosomes that were used for determination of p-EF2 levels and puromycin incorporation (Figure 5D). These studies showed that levels of ATP synthase β subunit protein are increased 30 min after stimulation of WT synaptosomes but are unchanged after stimulation of *Fmr1*$^{-/y}$ synaptosomes. Moreover, CsA treatment of the *Fmr1*$^{-/y}$ synaptosomes restored the normal stimulus-induced increase in β subunit protein (Figure 5D). Comparing column 3 to column 2 (in the last panel of Figure 5D) we find there is a markedly enhanced rate of *de novo* synthesis of β subunit protein at 30 min after peak EF2 phosphorylation, suggesting a rapid change in ATP synthase stoichiometry upon synaptic stimulation.

ATP Synthase Modulation Enhances Synaptic Plasticity

A number of studies have reported that FXS produces abnormalities in dendritic spines, including an increase in the number of spines and delays in their morphological maturity (for review, see He and Portera-Cailliau, 2013). To determine if ATP synthase leak closure rescues dendritic spine abnormalities, we carried out analyses of dendritic spine morphology in WT and FX neuronal cultures exposed to Dex or vehicle. In vehicle-treated WT cultures (at DIV 20), mushroom (mature) spines contributed ~50% of the total spine count, whereas in the FX cultures, mushroom spines represented only 10%. Dex treatment caused a 3-fold increase in the mature spines in FX cultures that increased the mature spines to 25% of the total spine count (Figures 6A–6F).

Dex, in addition to CsA, increases the efficiency in ATP production by ATP synthase (Alavian et al., 2015), which should phosphorylate targets such as EF2 during synaptic stimulation. To determine if local ATP levels are affected by stimulation in FX synapses, we measured ATP levels in living neurons using an ATP-fluorescence resonance energy transfer (FRET) construct (Imamura et al., 2009). We found that at 1 h after synaptic stimulation, ATP levels were decreased in FX synapses compared to WT. In contrast, treatment with Dex restored post-stimulation levels of ATP in FX synapses to those of WT (Figure 6G).

Dex Rescues Autistic Behaviors in the *Fmr1*$^{-/y}$ Mice

Developmental synaptic plasticity is required for normal mammalian behavior (Citri and Malenka, 2008). *Fmr1*$^{-/y}$ mice exhibit abnormal behaviors that can be measured by various paradigms. For example, they are more likely to engage in repetitive behaviors including grooming and shredding their nestlets (Angoa-Pérez et al., 2013; Kalueff et al., 2016; Kane et al., 2012; Silverman et al., 2010). *Fmr1*$^{-/y}$ mice are also hyperactive compared to WT mice, as measured by overall locomotor

(C) Dex decreases protein synthesis rate in FX neurons. Representative blot of puromycin incorporation in FX cortical cultures is shown in the presence of different concentrations of Dex. Cultures were treated with Dex for 2–24 h.
(D) Group data for experiments shown in (C). The group data for WT translation rates are shown in (H). n= samples from at least 3 independent cultures.
(E) Puromycin incorporation into WT and *Fmr1*$^{-/y}$ after incubation of mouse brain slices with 10 μM Dex or vehicle for 2.5 h.
(F) Group data of experiments shown in (E). n = 3–6 brain slices for each condition, at least three animals per condition.
(G) Representative immunoblot of puromycin incorporation showing that the rate of protein synthesis in FX cortical neurons is increased over WT neurons; exposure to 0.2 μM CsA for 7 days reduced the rate of puromycin incorporation in FX neurons.
(H) Quantification of the data shown in (G) n = samples from at least 3 independent cultures.
(I–M) Increase in rosettes (indicating actively translating ribosomes) in *Fmr1*$^{-/y}$ over WT brains is shown in these panels. The increase in rosettes is normalized in the *Fmr1*$^{-/y}$ brain to WT levels by CsA exposure. Representative electron micrographs of the CA1 region of hippocampal brain slices of *Fmr1*$^{-/y}$ mouse is shown and compared to WT and CsA exposed slices (R, ribosomal rosettes; M, mitochondria). (K) A higher magnification of the actively translating ribosomes (rosettes) shown in (J). Parallel slices from the corresponding hemisphere were incubated in 0.2 μM CsA or vehicle for 2.5 h. Scale bars as indicated.
(N) Group data of 65–76 micrographs analyzed per condition. (A) and (B) used unpaired two-tailed Student's t test. In (D), one-way ANOVA followed by Tukey's multiple comparisons test was used. For (F), (H), and (N), two-way ANOVA followed by Tukey's multiple comparisons test was used. Data are represented as mean ± SEM (*$p < 0.05$; **$p < 0.01$; ***$p < 0.001$; ****$p < 0.0001$).
See also Figure S2 and Table S2.

Please cite this article in press as: Licznerski et al., ATP Synthase c-Subunit Leak Causes Aberrant Cellular Metabolism in Fragile X Syndrome, Cell (2020), https://doi.org/10.1016/j.cell.2020.07.008

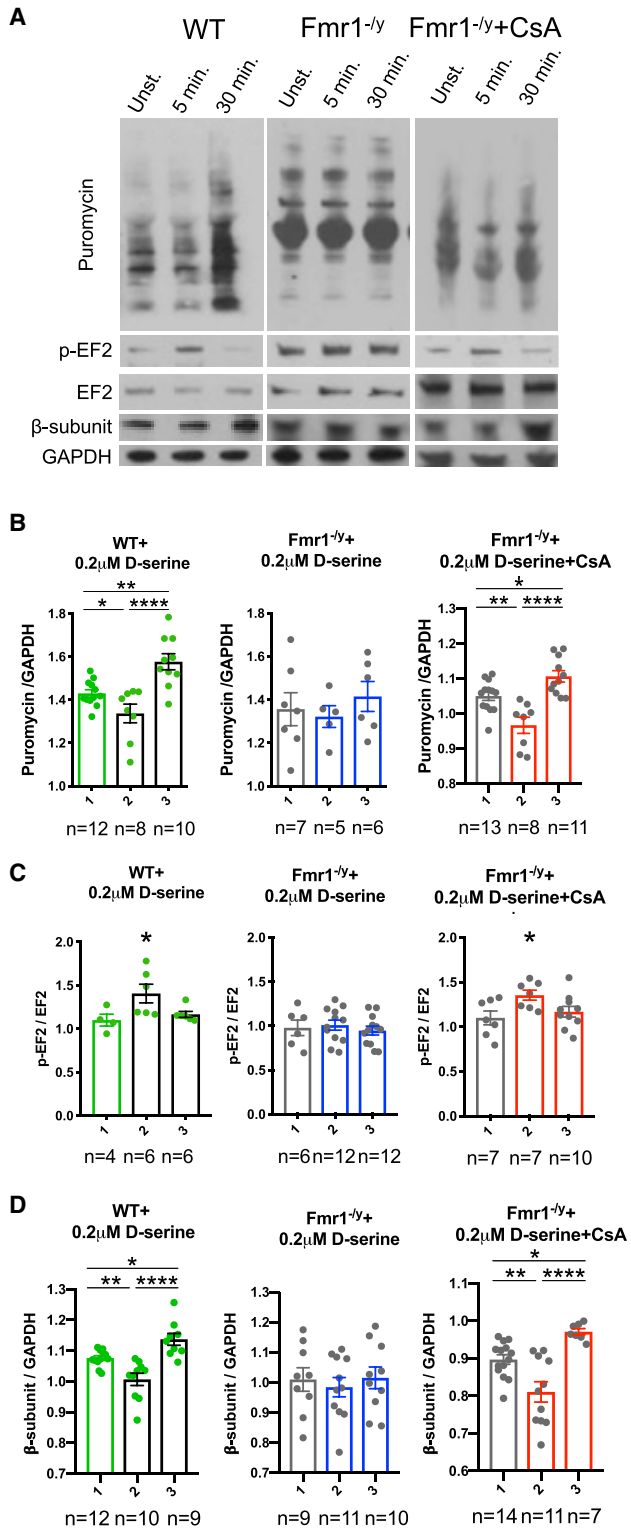

Figure 5. The Time Course of Synaptic Stimulation-Induced Changes in Protein Synthesis and EF2 Phosphorylation Is Disrupted in *Fmr1*$^{-/y}$ Synaptosomes, Normalized by ATP Synthase Leak Inhibition

(A) Representative immunoblots of synaptosomal samples harvested at the indicated time points before and after 0.2 μM D-serine stimulation. Top panels: puromycin incorporation; middle panels: p-EF2 and EF2; bottom panels: ATP synthase β subunit and protein loading control (GAPDH). CsA restores the normal pattern of response to stimulation in *Fmr1*$^{-/y}$ synaptosomes.

(B–D) Group data for experiments shown in (A): (B) for puromycin incorporation, (C) p-EF2/EF2 protein levels, and (D) ATP synthase β subunit protein levels. One-way ANOVA followed by Tukey's multiple comparisons test was used for all panels in the figure. Synaptosomes were prepared from at least three independent animals per condition. n= samples. Data are represented as mean ± SEM (*p < 0.05; **p < 0.01; ***p < 0.001; ****p < 0.0001).

See also Figure S1.

activity (Baker et al., 2010; Dolan et al., 2013; Tranfaglia, 2011). To determine if ATP synthase leak closure rescues these behavioral abnormalities, we injected 2-month-old mice with Dex over 2 days and tested their repetitive behaviors and locomotor activity. Although Dex did not significantly alter repetitive behaviors in WT mice, it markedly reduced the time spent grooming and the number of attempts made at grooming in *Fmr1*$^{-/y}$ animals (Figures 6H and 6I). Dex also decreased the abnormal nestlet shredding behavior measured in *Fmr1*$^{-/y}$ mice, suggesting that inhibiting the ATP synthase leak normalizes certain types of autistic behaviors (Figure 6J). Dex also markedly reduced the hyperactivity of *Fmr1*$^{-/y}$ mice (Figure 6K). The amelioration of these behavioral patterns by Dex suggests that ATP synthase leak inhibition is required for the development of normal mammalian behaviors.

DISCUSSION

We have found that the mitochondrial inner membrane leak of FX neurons and cells is caused by abnormal levels of ATP synthase c-subunit. The c-subunit leak causes persistence of a mitochondrial leak metabolic phenotype characterized by high glycolytic flux, high lactate levels, and increased levels of glycolytic and TCA enzymes. The leak also aberrantly elevates overall and specific protein synthesis; a decrease in c-subunit level or pharmacological inhibition of the ATP synthase leak reduces protein synthesis rates and decreases the levels of leak metabolism enzymes. In *Fmr1*$^{-/y}$ synapses, stimulation-dependent protein synthesis is absent. This is correlated with a lack of stimulus-induced EF2 phosphorylation and a lack of synthesis of the ATP synthase β-subunit. These abnormalities are readily reversed by ATP synthase leak inhibitors, suggesting that leak closure is required for the ATP-dependent phosphorylation of EF2 adjacent to mitochondria. EF2 phosphorylation may regulate the change in subsets of proteins synthesized and may be correlated with- the overabundant synthesis of enzymes supporting a high flux glycolytic/TCA cycle "leak" metabolism indicative of metabolic immaturity. Consistent with the hypothesis that the c-subunit leak is also a major cause of synapse immaturity, we find that inhibition of the ATP synthase leak allows the maturation of synapses and normalizes autistic behaviors.

ATP Synthase Leak Closure Regulates Metabolic and Synaptic Maturation in an FMRP-Dependent Manner

Our findings highlight the complex metabolic scenario of FMRP-deficient neurons. Normally there is an increase in synaptic/neuronal activity during early neuronal development (Bailey

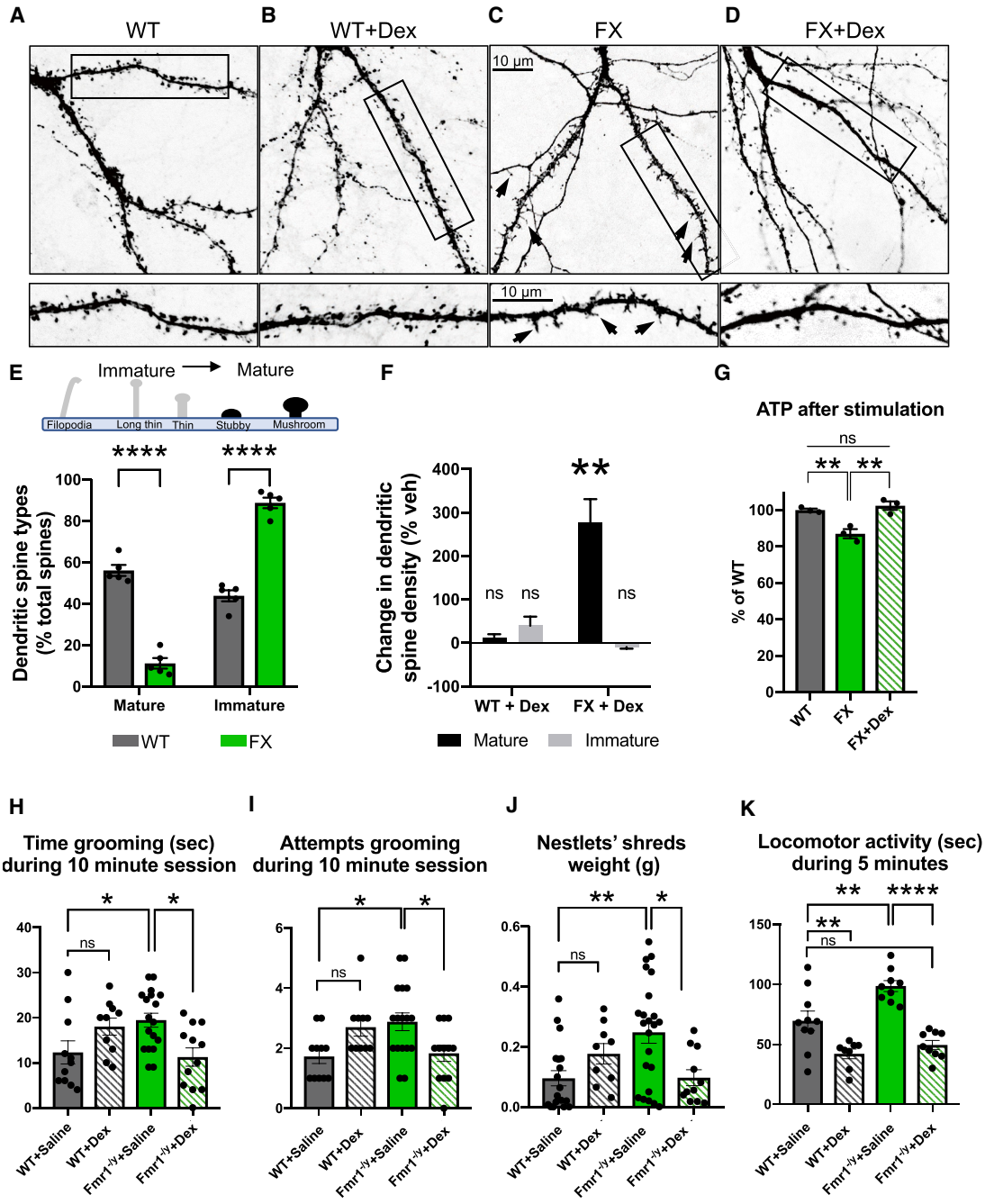

Figure 6. ATP Synthase Leak Inhibition Enhances Synaptic Plasticity

(A–D) Representative micrographs of primary neurons show the differences in synaptic spine morphology between FX and WT neurons. FX neurons (panel C) have fewer mature, mushroom-like spines compared to WT (panel A) but this is normalized by Dex (panel D). WT spine morphologies are unaffected by Dex (panel B). Insets show details of dendritic shafts.

(E) Dendritic spines were categorized according to their morphology into mature and immature spines. Illustration depicts subtypes of spines analyzed. Histograms show FX neurons have a reduced percentage of mature spines and an increased percentage of immature spines compared to WT. The types of spines are graphed as a percent of the total number of spines counted per unit length. n= 5 neurons per condition from at least 2 independent cultures.

(F) 5 μM Dex treatment each day for 6 consecutive days (DIV 15–20) caused an increase in the percent of mature dendritic spines / total spines per unit length in FX neurons. Dex treatment had no effect on WT neuron spine density. n= 5 neurons per condition from at least 2 independent cultures.

(G) Dex normalizes dendritic ATP levels in stimulated FX neurons. ATP levels were measured in neurons at DIV 20 using FRET-based ATP reporter ATeam YEMK. Neurons were stimulated for 3 min with 10 μM D-serine and ATP values were recorded at 1 h after stimulation. Histogram shows ATP values at 1 h after stimulation as a percentage of WT at 1 h after stimulation. n= 3 neurons per condition; 15–30 ROIs measured per neuron.

(legend continued on next page)

Please cite this article in press as: Licznerski et al., ATP Synthase c-Subunit Leak Causes Aberrant Cellular Metabolism in Fragile X Syndrome, Cell (2020), https://doi.org/10.1016/j.cell.2020.07.008

et al., 2015; Watson et al., 2016) accompanied by a change in metabolism from glycolytic to oxidative phosphorylation (Fame et al., 2019; Zheng et al., 2016). Our findings suggest persistence of a glycolytic/TCA cycle leak metabolic phenotype at the time of synapse formation in the FX neuronal cultures. Although it has been previously shown and is well-accepted that FMRP binds to synaptic mRNAs, the specific mRNAs that regulate synapse development are not known and how they contribute to development in an FMRP-dependent manner is not fully understood. The present results suggest that FMRP binds to ATP synthase β subunit mRNA to regulate the timing of metabolic maturation from a leak phenotype toward oxidative phosphorylation. It is not likely that the change in levels of glycolytic/TCA enzymes occurs by direct FMRP binding to the enzyme mRNAs. Only Hexokinase I is a possible FMRP target out of the group of metabolic enzymes that we find elevated by immunoblot (Darnell et al., 2011). Instead, when synaptic stimulation increases ATP synthase β subunit levels in an FMRP-dependent manner and closes the c-subunit leak, this may change the probability of translation of a subset of mRNAs waiting near the mitochondria, thereby changing levels of metabolic enzymes required for efficient oxidative phosphorylation and decreasing those needed for the leak metabolism. Of course, it is also possible that stimulation might release FMRP from a metabolic transcriptional regulator (Fame et al., 2019), thereby coordinating the decrease in glycolytic/TCA enzymes with the increase in ATP synthase enzyme components. Future analysis will discover which scenario is tractable.

ATP Synthase c-Subunit Leak Channel Regulates the Rate of Protein Synthesis in FX Neurons and Fibroblasts

One of the key findings of this study is that the ATP synthase c-subunit leak channel level activity regulates the rate of protein synthesis. We demonstrate that knock down or overexpression of the c-subunit directly regulates the rate of protein synthesis measured by puromycin incorporation. Pharmacological reagents Dex and CsA that bind within the ATP synthase F_1 to reduce c-subunit leak channel activity (Alavian et al., 2011, 2015; Chen et al., 2011; Giorgio et al., 2009; Szabó and Zoratti, 1991) also reduce overall protein synthesis. Finally, Bcl-xL, a protein that we have reported previously to bind to the F_1 (Alavian et al., 2011; Chen et al., 2011), reduces protein synthesis, suggesting that Bcl-xL or another endogenous ATP synthase leak modulator (Stefely and Pagliarini, 2017) could also assist in the stimulus-dependent changes in protein synthesis (Figures S2F–S2H). We find that the reason the leak is so important for regulation of the rate of protein synthesis is because the increase in mitochondrial ATP produced by leak closure is used in phosphorylating local translation targets. We identified EF2, because its rapid phosphorylation after high intensity glutamate receptor stimulation (Scheetz et al., 2000) suggested it as a candidate to produce a change in synaptic plasticity. Indeed, we found that there was no phosphorylation of EF2 or change in rate of protein synthesis in *Fmr1*$^{-/y}$ synapses after glutamate receptor stimulation. In contrast, the stimulus-dependent phosphorylation event was rescued by closing the ATP synthase leak with CsA (Giorgio et al., 2009; Szabó and Zoratti, 1991).

Mitochondrial Inner Membrane Leak Closure Decreases "Leak" Metabolism, Favoring More Efficient Oxidative Phosphorylation during Synaptogenesis

Immature cells prefer a metabolism favoring glycolytic production of ATP over mitochondrial ATP production (Warburg, 1956; Zheng et al., 2016), but the idea that a shift toward oxidative phosphorylation could occur during synaptogenesis has not been shown previously. Recent reports in cardiomyocytes support this developmental shift. Cardiomyocytes change their metabolism (from glycolytic to oxidative) over several days during embryonic development (Hom et al., 2011). The respiratory complexes aggregate into a "supercomplex" (Beutner et al., 2017). These events occur earlier in cells that have been exposed to CsA (Hom et al., 2011). Studies also support a similar scenario in early neuronal differentiation from stem cells (Fame et al., 2019; Zheng et al., 2016). Our previous work has suggested that oxidative changes in synapses during development are regulated by increases in expression of the anti-apoptotic protein Bcl-xL. Bcl-xL levels peak during periods of synaptogenesis in the developing brain, then remain elevated in adulthood (Krajewska et al., 2002). We have reported that overexpression of Bcl-xL enhances synapse formation and maturity in hippocampal neurons (Li et al., 2008). Bcl-xL supports both mitochondrial biogenesis and movement of mitochondria closer to synaptic sites during synaptic enlargement (Berman et al., 2009; Li et al., 2008). Accompanying this change is an improvement in the efficiency of oxidative phosphorylation as Bcl-xL interacts directly with the ATP synthase F_1 to improve enzymatic function and close the inner membrane leak (Alavian et al., 2011; Chen et al., 2011).

Unlike for cardiomyocytes as described above, at the same embryonic dates (~E9), oxygen consumption is high in the developing nervous system yet accompanied by high glycolytic flux. Different from the heart, oxygen consumption then actually decreases upon neuronal maturation as oxidative phosphorylation takes over as the main metabolic phenotype (Fame et al., 2019). Recent accounts have highlighted that metabolic phenotypes are much more complex than simply "glycolytic" versus "oxidative," and mitochondria are not always silent when glycolytic metabolism is favored (Li et al., 2016; Vander Heiden et al., 2009; Zheng et al., 2016). On the contrary, mitochondrial metabolism is often enhanced in that use of the TCA cycle for anabolism is increased; this includes upregulation of enzymes needed for lipid biosynthesis, protein synthesis and deoxy- and ribonucleic acid biosynthesis. Hallmarks of this state are the upregulation of enzymes involved in glutaminolysis (Wise et al., 2008),

(H–K) Abnormal behavior in *Fmr1*$^{-/y}$ mice is rescued by Dex. Two-month-old mice were given 3 intraperitoneal injections of 10 mg/kg Dex or saline over 40 h prior to behavioral testing. Repetitive behaviors (grooming and nestlet shredding, H–I) were normalized by Dex in *Fmr1*$^{-/y}$ mice. Hyperactivity (K) as measured by locomotor activity was normalized by Dex in *Fmr1*$^{-/y}$ mice. In (E) and (F), unpaired two-tailed Student's t test was used. For (G), one-way ANOVA followed by Tukey's multiple comparisons test was used. For (H)–(K), two-way ANOVA followed by Tukey's multiple comparisons test was used. Data are represented as mean ± SEM (*$p < 0.05$; **$p < 0.01$; ***$p < 0.001$; ****$p < 0.0001$).

malate aspartate shuttle (Li et al., 2016), the re-supply of NAD^+, alteration of the NAD^+/NADH ratio (Magni et al., 2008), and changes in pyruvate metabolism (Dayton et al., 2016). Enzymes upregulated for this form of metabolism include lactate dehydrogenase, malate dehydrogenase, glutamate dehydrogenase, isocitrate dehydrogenase, and PKM2 (Dayton et al., 2016). In our current study, the list of enzymes that are upregulated in FX versus WT neurons and synapses includes all the pathways mentioned above. Most strikingly, these are rapidly downregulated in FX neurons following Dex treatment, suggesting high metabolic flexibility in early developing neurons and synapses. These results also suggest that inner membrane leak may be upregulated early in development to enhance electron transport so that NAD^+ can be reformed from NADH. In addition, the TCA cycle may run faster in the presence of an inner membrane leak to synthesize components of developing cells/synapses. It is likely that this "leak" metabolic phenotype is advantageous to FX neurons, because they require increased protein synthesis and may need enhanced lipid supply for membrane remodeling. This is supported by several recent reports including in *dfmr1* mutant mitochondria in which it was described that mitochondria have significantly increased maximum electron transport system (ETS) capacity accompanied by high oxygen consumption, reduced carbohydrate and lipid stores and hyperphagia, suggestive of an inner mitochondrial membrane leak (Weisz et al., 2018). NAD^+/NADH ratio was also significantly lower in the *dfmr1* mutants relative to controls (Weisz et al., 2018), suggesting the requirement for upregulation of enzymes that resupply NAD^+. A recent report on *Fmr1*$^{-/y}$ mouse brains shows that electron transport complexes run at high rates even though mitochondrial ATP production is low, suggesting inner membrane inefficiency (D'Antoni et al., 2020). Our recent findings confirm that mitochondria from the *Fmr1*$^{-/y}$ mouse brains have inefficient and membrane potential-dependent enhancement in oxygen consumption caused by an inner membrane leak sensitive to coenzyme Q and CsA (Griffiths et al., 2020). Therefore, the "leak" metabolism of neuronal immaturity in our analysis of these examples is characterized by high glycolytic/TCA flux and high electron transport with an increase, not a decrease, in oxygen consumption.

Although we have been concentrating on the leak as the abnormality in this study, the ATP synthase is only one part of a complex inner mitochondrial membrane structure (Cogliati et al., 2016; Davies et al., 2012). Changes in cristae morphology at the onset of oxidative metabolism contribute to the enhanced efficiency of ATP production (Esparza-Perusquía et al., 2017). These alterations in mitochondrial inner membrane architecture may occur during normal synaptic maturation, suggesting other ways in which mitochondrial plasticity may be required for mature synapse formation.

STAR★METHODS

Detailed methods are provided in the online version of this paper and include the following:

SUPPLEMENTAL INFORMATION

Supplemental Information can be found online at https://doi.org/10.1016/j.cell.2020.07.008.

ACKNOWLEDGMENTS

The Q-Exactive Plus mass spectrometer located at the Yale/Keck MS & Proteomics Resource where the mass spectrometry work was carried out was funded in part by NIH SIG from the Office of The Director, NIH (S10OD018034). The content is solely the responsibility of the authors and does not necessarily represent the official views of the NIH. We also would like to thank Weiwei Wang and Jean Kanyo for assistance with mass spectrometry, sample preparation and data collection; and Dr. TuKiet Lam for his help with interpreting the data. Human FX and WT cell lines were kindly shared by Dr. Gary J. Bassell laboratory (Emory University, Atlanta, GA) and Dr. Elizabeth Berry-Kravis (Rush University Medical Center, Chicago, IL). We also thank Dr. Leonard K. Kaczmarek (Yale University, New Haven, CT) for sharing FVB and FMRP KO mice and for insightful scientific discussion. FRET constructs were kindly provided by Dr. Imamura and Dr. Noji (Imamura et al., 2009).

This study was supported by FRAXA, Simons Foundation, NIH NS112706 and NIH NS045876 (to E.A.J.), NIA (K01AG054734 to N. Mnatsakanyan),

Beavers Award and NSF Research Experiences for Undergraduates (REU) (to L.B.), Yale College First-Year Summer Research Fellowship in the Sciences and Engineering (to G.N.X.), Yale College STARS I Summer Research Program (to A.B.), NSF REU (to N.C.-R.), METCALF Internship from the University of Chicago (to N. Mehta, S.S., J.S., and E.S.).

AUTHOR CONTRIBUTIONS

P.L. and E.A.J. conceived the project, designed experiments, interpreted the data and prepared the manuscript. P.L., H.P., H.R., R.C., P.M., N. Mnatsakanyan, M.G., J.W., N.C.-R., N. Mehta, S.S., J.S., E.S., C.E., S.E., L.B., G.N.X., A.B., V.K.G., and E.A.J. performed experiments. V.K.G. and R.J.L. provided scientific discussion and intellectual contributions.

DECLARATION OF INTERESTS

The authors declare no competing interests.

Received: November 14, 2018
Revised: March 4, 2020
Accepted: July 10, 2020
Published: August 13, 2020

REFERENCES

Alavian, K.N., Li, H., Collis, L., Bonanni, L., Zeng, L., Sacchetti, S., Lazrove, E., Nabili, P., Flaherty, B., Graham, M., et al. (2011). Bcl-xL regulates metabolic efficiency of neurons through interaction with the mitochondrial F1FO ATP synthase. Nat. Cell Biol. *13*, 1224–1233.

Alavian, K.N., Beutner, G., Lazrove, E., Sacchetti, S., Park, H.A., Licznerski, P., Li, H., Nabili, P., Hockensmith, K., Graham, M., et al. (2014). An uncoupling channel within the c-subunit ring of the F1FO ATP synthase is the mitochondrial permeability transition pore. Proc. Natl. Acad. Sci. USA *111*, 10580–10585.

Alavian, K.N., Dworetzky, S.I., Bonanni, L., Zhang, P., Sacchetti, S., Li, H., Signore, A.P., Smith, P.J., Gribkoff, V.K., and Jonas, E.A. (2015). The mitochondrial complex V-associated large-conductance inner membrane current is regulated by cyclosporine and dexpramipexole. Mol. Pharmacol. *87*, 1–8.

Angoa-Pérez, M., Kane, M.J., Briggs, D.I., Francescutti, D.M., and Kuhn, D.M. (2013). Marble burying and nestlet shredding as tests of repetitive, compulsive-like behaviors in mice. J. Vis. Exp. (82), 50978.

Autry, A.E., and Monteggia, L.M. (2012). Brain-derived neurotrophic factor and neuropsychiatric disorders. Pharmacol. Rev. *64*, 238–258.

Bagni, C., and Greenough, W.T. (2005). From mRNP trafficking to spine dysmorphogenesis: the roots of fragile X syndrome. Nat. Rev. Neurosci. *6*, 376–387.

Bailey, C.H., Kandel, E.R., and Harris, K.M. (2015). Structural Components of Synaptic Plasticity and Memory Consolidation. Cold Spring Harb. Perspect. Biol. *7*, a021758.

Baines, C.P., Kaiser, R.A., Purcell, N.H., Blair, N.S., Osinska, H., Hambleton, M.A., Brunskill, E.W., Sayen, M.R., Gottlieb, R.A., Dorn, G.W., et al. (2005). Loss of cyclophilin D reveals a critical role for mitochondrial permeability transition in cell death. Nature *434*, 658–662.

Baker, K.B., Wray, S.P., Ritter, R., Mason, S., Lanthorn, T.H., and Savelieva, K.V. (2010). Male and female Fmr1 knockout mice on C57 albino background exhibit spatial learning and memory impairments. Genes Brain Behav. *9*, 562–574.

Bassell, G.J., and Warren, S.T. (2008). Fragile X syndrome: loss of local mRNA regulation alters synaptic development and function. Neuron *60*, 201–214.

Bear, M.F., Huber, K.M., and Warren, S.T. (2004). The mGluR theory of fragile X mental retardation. Trends Neurosci. *27*, 370–377.

Beaudoin, G.M., 3rd, Lee, S.H., Singh, D., Yuan, Y., Ng, Y.G., Reichardt, L.F., and Arikkath, J. (2012). Culturing pyramidal neurons from the early postnatal mouse hippocampus and cortex. Nat. Protoc. *7*, 1741–1754.

Berman, S.B., Chen, Y.B., Qi, B., McCaffery, J.M., Rucker, E.B., 3rd, Goebbels, S., Nave, K.A., Arnold, B.A., Jonas, E.A., Pineda, F.J., and Hardwick, J.M. (2009). Bcl-x L increases mitochondrial fission, fusion, and biomass in neurons. J. Cell Biol. *184*, 707–719.

Bernardi, P., and Di Lisa, F. (2015). The mitochondrial permeability transition pore: Molecular nature and role as a target in cardioprotection. J. Mol. Cell. Cardiol. *78*, 100–106.

Beutner, G., Eliseev, R.A., and Porter, G.A., Jr. (2014). Initiation of electron transport chain activity in the embryonic heart coincides with the activation of mitochondrial complex 1 and the formation of supercomplexes. PLoS ONE *9*, e113330.

Beutner, G., Alanzalon, R.E., and Porter, G.A., Jr. (2017). Cyclophilin D regulates the dynamic assembly of mitochondrial ATP synthase into synthasomes. Sci. Rep. *7*, 14488.

Bhattacharya, A., Kaphzan, H., Alvarez-Dieppa, A.C., Murphy, J.P., Pierre, P., and Klann, E. (2012). Genetic removal of p70 S6 kinase 1 corrects molecular, synaptic, and behavioral phenotypes in fragile X syndrome mice. Neuron *76*, 325–337.

Bonora, M., Bononi, A., De Marchi, E., Giorgi, C., Lebiedzinska, M., Marchi, S., Patergnani, S., Rimessi, A., Suski, J.M., Wojtala, A., et al. (2013). Role of the c subunit of the FO ATP synthase in mitochondrial permeability transition. Cell Cycle *12*, 674–683.

Bozik, M.E., Kramer, W.G., Gribkoff, V.K., and Ingersoll, E.W. (2010). Safety, Tolerability, and Pharmacokinetics of KNS-760704 (Dexpramipexole) in Healthy Adult Subjects. J. Clin. Pharmacol. https://doi.org/10.1177/0091270010379412.

Bozik, M.E., Mather, J.L., Kramer, W.G., Gribkoff, V.K., and Ingersoll, E.W. (2011). Safety, tolerability, and pharmacokinetics of KNS-760704 (dexpramipexole) in healthy adult subjects. J. Clin. Pharmacol. *51*, 1177–1185.

Brandt, T., Mourier, A., Tain, L.S., Partridge, L., Larsson, N.G., and Kühlbrandt, W. (2017). Changes of mitochondrial ultrastructure and function during ageing in mice and *Drosophila*. eLife *6*, e24662.

Brown, M.R., Sullivan, P.G., Dorenbos, K.A., Modafferi, E.A., Geddes, J.W., and Steward, O. (2004). Nitrogen disruption of synaptoneurosomes: an alternative method to isolate brain mitochondria. J. Neurosci. Methods *137*, 299–303.

Brown, M.R., Kronengold, J., Gazula, V.R., Chen, Y., Strumbos, J.G., Sigworth, F.J., Navaratnam, D., and Kaczmarek, L.K. (2010). Fragile X mental retardation protein controls gating of the sodium-activated potassium channel Slack. Nat. Neurosci. *13*, 819–821.

Caviston, T.L., Ketchum, C.J., Sorgen, P.L., Nakamoto, R.K., and Cain, B.D. (1998). Identification of an uncoupling mutation affecting the b subunit of F1F0 ATP synthase in Escherichia coli. FEBS Lett. *429*, 201–206.

Chan, T.L., Greenawalt, J.W., and Pedersen, P.L. (1970). Biochemical and ultrastructural properties of a mitochondrial inner membrane fraction deficient in outer membrane and matrix activities. J. Cell Biol. *45*, 291–305.

Chen, C., Ko, Y., Delannoy, M., Ludtke, S.J., Chiu, W., and Pedersen, P.L. (2004). Mitochondrial ATP synthasome: three-dimensional structure by electron microscopy of the ATP synthase in complex formation with carriers for Pi and ADP/ATP. J. Biol. Chem. *279*, 31761–31768.

Chen, Y.B., Aon, M.A., Hsu, Y.T., Soane, L., Teng, X., McCaffery, J.M., Cheng, W.C., Qi, B., Li, H., Alavian, K.N., et al. (2011). Bcl-xL regulates mitochondrial energetics by stabilizing the inner membrane potential. J. Cell Biol. *195*, 263–276.

Chen, R., Park, H.A., Mnatsakanyan, N., Niu, Y., Licznerski, P., Wu, J., Miranda, P., Graham, M., Tang, J., Boon, A.J.W., et al. (2019). Parkinson's disease protein DJ-1 regulates ATP synthase protein components to increase neuronal process outgrowth. Cell Death Dis. *10*, 469.

Citri, A., and Malenka, R.C. (2008). Synaptic plasticity: multiple forms, functions, and mechanisms. Neuropsychopharmacology *33*, 18–41.

Cogliati, S., Enriquez, J.A., and Scorrano, L. (2016). Mitochondrial Cristae: Where Beauty Meets Functionality. Trends Biochem. Sci. *41*, 261–273.

Cudkowicz, M., Bozik, M.E., Ingersoll, E.W., Miller, R., Mitsumoto, H., Shefner, J., Moore, D.H., Schoenfeld, D., Mather, J.L., Archibald, D., et al. (2011). The effects of dexpramipexole (KNS-760704) in individuals with amyotrophic lateral sclerosis. Nat. Med. *17*, 1652–1656.

D'Antoni, S., de Bari, L., Valenti, D., Borro, M., Bonaccorso, C.M., Simmaco, M., Vacca, R.A., and Catania, M.V. (2020). Aberrant mitochondrial bioenergetics in the cerebral cortex of the Fmr1 knockout mouse model of fragile X syndrome. Biol. Chem. *401*, 497–503.

Darnell, J.C. (2011). Defects in translational regulation contributing to human cognitive and behavioral disease. Curr. Opin. Genet. Dev. *21*, 465–473.

Darnell, J.C., Van Driesche, S.J., Zhang, C., Hung, K.Y., Mele, A., Fraser, C.E., Stone, E.F., Chen, C., Fak, J.J., Chi, S.W., et al. (2011). FMRP stalls ribosomal translocation on mRNAs linked to synaptic function and autism. Cell *146*, 247–261.

Davies, K.M., Anselmi, C., Wittig, I., Faraldo-Gómez, J.D., and Kühlbrandt, W. (2012). Structure of the yeast F1Fo-ATP synthase dimer and its role in shaping the mitochondrial cristae. Proc. Natl. Acad. Sci. USA *109*, 13602–13607.

Dayton, T.L., Jacks, T., and Vander Heiden, M.G. (2016). PKM2, cancer metabolism, and the road ahead. EMBO Rep. *17*, 1721–1730.

Deng, P.Y., Rotman, Z., Blundon, J.A., Cho, Y., Cui, J., Cavalli, V., Zakharenko, S.S., and Klyachko, V.A. (2013). FMRP regulates neurotransmitter release and synaptic information transmission by modulating action potential duration via BK channels. Neuron *77*, 696–711.

Dhillon, S., Hellings, J.A., and Butler, M.G. (2011). Genetics and mitochondrial abnormalities in autism spectrum disorders: a review. Curr. Genomics *12*, 322–332.

Dolan, B.M., Duron, S.G., Campbell, D.A., Vollrath, B., Shankaranarayana Rao, B.S., Ko, H.Y., Lin, G.G., Govindarajan, A., Choi, S.Y., and Tonegawa, S. (2013). Rescue of fragile X syndrome phenotypes in Fmr1 KO mice by the small-molecule PAK inhibitor FRAX486. Proc. Natl. Acad. Sci. USA *110*, 5671–5676.

Dölen, G., Osterweil, E., Rao, B.S., Smith, G.B., Auerbach, B.D., Chattarji, S., and Bear, M.F. (2007). Correction of fragile X syndrome in mice. Neuron *56*, 955–962.

Dölen, G., Carpenter, R.L., Ocain, T.D., and Bear, M.F. (2010). Mechanism-based approaches to treating fragile X. Pharmacol. Ther. *127*, 78–93.

El-Hassar, L., Song, L., Tan, W.J.T., Large, C.H., Alvaro, G., Santos-Sacchi, J., and Kaczmarek, L.K. (2019). Modulators of Kv3 Potassium Channels Rescue the Auditory Function of Fragile X Mice. J. Neurosci. *39*, 4797–4813.

Esparza-Perusquía, M., Olvera-Sánchez, S., Pardo, J.P., Mendoza-Hernández, G., Martínez, F., and Flores-Herrera, O. (2017). Structural and kinetics characterization of the F_1F_0-ATP synthase dimer. New repercussion of monomer-monomer contact. Biochim. Biophys. Acta Bioenerg. *1858*, 975–981.

Fame, R.M., Shannon, M.L., Chau, K.F., Head, J.P., and Lehtinen, M.K. (2019). A concerted metabolic shift in early forebrain alters the CSF proteome and depends on MYC downregulation for mitochondrial maturation. Development *146*, dev182857.

Gerle, C. (2016). On the structural possibility of pore-forming mitochondrial FoF1 ATP synthase. Biochim. Biophys. Acta *1857*, 1191–1196.

Gildish, I., Manor, D., David, O., Sharma, V., Williams, D., Agarwala, U., Wang, X., Kenney, J.W., Proud, C.G., and Rosenblum, K. (2012). Impaired associative taste learning and abnormal brain activation in kinase-defective eEF2K mice. Learn. Mem. *19*, 116–125.

Giorgio, V., Bisetto, E., Soriano, M.E., Dabbeni-Sala, F., Basso, E., Petronilli, V., Forte, M.A., Bernardi, P., and Lippe, G. (2009). Cyclophilin D modulates mitochondrial F0F1-ATP synthase by interacting with the lateral stalk of the complex. J. Biol. Chem. *284*, 33982–33988.

Giorgio, V., von Stockum, S., Antoniel, M., Fabbro, A., Fogolari, F., Forte, M., Glick, G.D., Petronilli, V., Zoratti, M., Szabó, I., et al. (2013). Dimers of mitochondrial ATP synthase form the permeability transition pore. Proc. Natl. Acad. Sci. USA *110*, 5887–5892.

Glass, L.N., Swapna, G., Chavadi, S.S., Tufariello, J.M., Mi, K., Drumm, J.E., Lam, T.T., Zhu, G., Zhan, C., Vilchéze, C., et al. (2017). Mycobacterium tuberculosis universal stress protein Rv2623 interacts with the putative ATP binding cassette (ABC) transporter Rv1747 to regulate mycobacterial growth. PLoS Pathog. *13*, e1006515.

Goh, S., Dong, Z., Zhang, Y., DiMauro, S., and Peterson, B.S. (2014). Mitochondrial dysfunction as a neurobiological subtype of autism spectrum disorder: evidence from brain imaging. JAMA Psychiatry *71*, 665–671.

Griffiths, K.K., Wang, A., Wang, L., Tracey, M., Kleiner, G., Quinzii, C.M., Sun, L., Yang, G., Perez-Zoghbi, J.F., Licznerski, P., et al. (2020). Inefficient thermogenic mitochondrial respiration due to futile proton leak in a mouse model of fragile X syndrome. FASEB J. *34*, 7404–7426.

Gu, J., Zhang, L., Zong, S., Guo, R., Liu, T., Yi, J., Wang, P., Zhuo, W., and Yang, M. (2019). Cryo-EM structure of the mammalian ATP synthase tetramer bound with inhibitory protein IF1. Science *364*, 1068–1075.

He, C.X., and Portera-Cailliau, C. (2013). The trouble with spines in fragile X syndrome: density, maturity and plasticity. Neuroscience *251*, 120–128.

Hom, J.R., Quintanilla, R.A., Hoffman, D.L., de Mesy Bentley, K.L., Molkentin, J.D., Sheu, S.S., and Porter, G.A., Jr. (2011). The permeability transition pore controls cardiac mitochondrial maturation and myocyte differentiation. Dev. Cell *21*, 469–478.

Imamura, H., Nhat, K.P., Togawa, H., Saito, K., Iino, R., Kato-Yamada, Y., Nagai, T., and Noji, H. (2009). Visualization of ATP levels inside single living cells with fluorescence resonance energy transfer-based genetically encoded indicators. Proc. Natl. Acad. Sci. USA *106*, 15651–15656.

Jacquemont, S., Pacini, L., Jønch, A.E., Cencelli, G., Rozenberg, I., He, Y., D'Andrea, L., Pedini, G., Eldeeb, M., Willemsen, R., et al. (2018). Protein synthesis levels are increased in a subset of individuals with fragile X syndrome. Hum. Mol. Genet. *27*, 2039–2051.

Kaech, S., and Banker, G. (2006). Culturing hippocampal neurons. Nat. Protoc. *1*, 2406–2415.

Kalueff, A.V., Stewart, A.M., Song, C., Berridge, K.C., Graybiel, A.M., and Fentress, J.C. (2016). Neurobiology of rodent self-grooming and its value for translational neuroscience. Nat. Rev. Neurosci. *17*, 45–59.

Kane, M.J., Angoa-Peréz, M., Briggs, D.I., Sykes, C.E., Francescutti, D.M., Rosenberg, D.R., and Kuhn, D.M. (2012). Mice genetically depleted of brain serotonin display social impairments, communication deficits and repetitive behaviors: possible relevance to autism. PLoS ONE *7*, e48975.

Kaplan, E.S., Cao, Z., Hulsizer, S., Tassone, F., Berman, R.F., Hagerman, P.J., and Pessah, I.N. (2012). Early mitochondrial abnormalities in hippocampal neurons cultured from Fmr1 pre-mutation mouse model. J. Neurochem. *123*, 613–621.

Klemmer, P., Meredith, R.M., Holmgren, C.D., Klychnikov, O.I., Stahl-Zeng, J., Loos, M., van der Schors, R.C., Wortel, J., de Wit, H., Spijker, S., et al. (2011). Proteomics, ultrastructure, and physiology of hippocampal synapses in a fragile X syndrome mouse model reveal presynaptic phenotype. J. Biol. Chem. *286*, 25495–25504.

Ko, Y.H., Delannoy, M., Hullihen, J., Chiu, W., and Pedersen, P.L. (2003). Mitochondrial ATP synthasome. Cristae-enriched membranes and a multiwell detergent screening assay yield dispersed single complexes containing the ATP synthase and carriers for Pi and ADP/ATP. J. Biol. Chem. *278*, 12305–12309.

Krajewska, M., Mai, J.K., Zapata, J.M., Ashwell, K.W., Schendel, S.L., Reed, J.C., and Krajewski, S. (2002). Dynamics of expression of apoptosis-regulatory proteins Bid, Bcl-2, Bcl-X, Bax and Bak during development of murine nervous system. Cell Death Differ. *9*, 145–157.

Li, H., Chen, Y., Jones, A.F., Sanger, R.H., Collis, L.P., Flannery, R., McNay, E.C., Yu, T., Schwarzenbacher, R., Bossy, B., et al. (2008). Bcl-xL induces Drp1-dependent synapse formation in cultured hippocampal neurons. Proc. Natl. Acad. Sci. USA *105*, 2169–2174.

Li, H., Alavian, K.N., Lazrove, E., Mehta, N., Jones, A., Zhang, P., Licznerski, P., Graham, M., Uo, T., Guo, J., et al. (2013). A Bcl-xL-Drp1 complex regulates synaptic vesicle membrane dynamics during endocytosis. Nat. Cell Biol. *15*, 773–785.

Li, C., Zhang, G., Zhao, L., Ma, Z., and Chen, H. (2016). Metabolic reprogramming in cancer cells: glycolysis, glutaminolysis, and Bcl-2 proteins as novel therapeutic targets for cancer. World J. Surg. Oncol. *14*, 15.

Lumaban, J.G., and Nelson, D.L. (2015). The Fragile X proteins Fmrp and Fxr2p cooperate to regulate glucose metabolism in mice. Hum. Mol. Genet. *24*, 2175–2184.

Magni, G., Orsomando, G., Raffelli, N., and Ruggieri, S. (2008). Enzymology of mammalian NAD metabolism in health and disease. Front. Biosci. *13*, 6135–6154.

McCarron, J.G., Wilson, C., Sandison, M.E., Olson, M.L., Girkin, J.M., Saunter, C., and Chalmers, S. (2013). From structure to function: mitochondrial morphology, motion and shaping in vascular smooth muscle. J. Vasc. Res. *50*, 357–371.

McCullagh, E.A., Rotschafer, S.E., Auerbach, B.D., Klug, A., Kaczmarek, L.K., Cramer, K.S., Kulesza, R.J., Jr., Razak, K.A., Lovelace, J.W., Lu, Y., et al. (2020). Mechanisms underlying auditory processing deficits in Fragile X syndrome. FASEB J. *34*, 3501–3518.

Mnatsakanyan, N., and Jonas, E.A. (2020). ATP synthase c-subunit ring as the channel of mitochondrial permeability transition: Regulator of metabolism in development and degeneration. J. Mol. Cell. Cardiol. *144*, 109–118.

Mnatsakanyan, N., Llaguno, M.C., Yang, Y., Yan, Y., Weber, J., Sigworth, F.J., and Jonas, E.A. (2019). A mitochondrial megachannel resides in monomeric F_1F_O ATP synthase. Nat. Commun. *10*, 5823.

Muscas, M., Louros, S.R., and Osterweil, E.K. (2019). Lovastatin, not Simvastatin, Corrects Core Phenotypes in the Fragile X Mouse Model. eNeuro *6*, ENEURO.0097-19.2019.

Muzzi, M., Gerace, E., Buonvicino, D., Coppi, E., Resta, F., Formentini, L., Zecchi, R., Tigli, L., Guasti, D., Ferri, M., et al. (2018). Dexpramipexole improves bioenergetics and outcome in experimental stroke. Br. J. Pharmacol. *175*, 272–283.

Nakagawa, T., Shimizu, S., Watanabe, T., Yamaguchi, O., Otsu, K., Yamagata, H., Inohara, H., Kubo, T., and Tsujimoto, Y. (2005). Cyclophilin D-dependent mitochondrial permeability transition regulates some necrotic but not apoptotic cell death. Nature *434*, 652–658.

Neginskaya, M.A., Solesio, M.E., Berezhnaya, E.V., Amodeo, G.F., Mnatsakanyan, N., Jonas, E.A., and Pavlov, E.V. (2019). ATP Synthase C-Subunit-Deficient Mitochondria Have a Small Cyclosporine A-Sensitive Channel, but Lack the Permeability Transition Pore. Cell Rep. *26*, 11–17.

Ofengeim, D., Chen, Y.B., Miyawaki, T., Li, H., Sacchetti, S., Flannery, R.J., Alavian, K.N., Pontarelli, F., Roelofs, B.A., Hickman, J.A., et al. (2012). N-terminally cleaved Bcl-xL mediates ischemia-induced neuronal death. Nat. Neurosci. *15*, 574–580.

Park, S., Park, J.M., Kim, S., Kim, J.A., Shepherd, J.D., Smith-Hicks, C.L., Chowdhury, S., Kaufmann, W., Kuhl, D., Ryazanov, A.G., et al. (2008). Elongation factor 2 and fragile X mental retardation protein control the dynamic translation of Arc/Arg3.1 essential for mGluR-LTD. Neuron *59*, 70–83.

Pfeiffer, B.E., and Huber, K.M. (2009). The state of synapses in fragile X syndrome. Neuroscientist *15*, 549–567.

Pyronneau, A., He, Q., Hwang, J.Y., Porch, M., Contractor, A., and Zukin, R.S. (2017). Aberrant Rac1-cofilin signaling mediates defects in dendritic spines, synaptic function, and sensory perception in fragile X syndrome. Sci. Signal. *10*, eaan0852.

Rasola, A., and Bernardi, P. (2014). The mitochondrial permeability transition pore and its adaptive responses in tumor cells. Cell Calcium *56*, 437–445.

Roberts, D.J., and Miyamoto, S. (2015). Hexokinase II integrates energy metabolism and cellular protection: Akting on mitochondria and TORCing to autophagy. Cell Death Differ. *22*, 364.

Sacchetti, S., Alavian, K.N., Lazrove, E., and Jonas, E.A. (2013). F1FO ATPase vesicle preparation and technique for performing patch clamp recordings of submitochondrial vesicle membranes. J. Vis. Exp. (75), e4394.

Santos, A.R., Kanellopoulos, A.K., and Bagni, C. (2014). Learning and behavioral deficits associated with the absence of the fragile X mental retardation protein: what a fly and mouse model can teach us. Learn. Mem. *21*, 543–555.

Scheetz, A.J., Nairn, A.C., and Constantine-Paton, M. (2000). NMDA receptor-mediated control of protein synthesis at developing synapses. Nat. Neurosci. *3*, 211–216.

Schmidt, E.K., Clavarino, G., Ceppi, M., and Pierre, P. (2009). SUnSET, a nonradioactive method to monitor protein synthesis. Nat. Methods *6*, 275–277.

Sidorov, M.S., Auerbach, B.D., and Bear, M.F. (2013). Fragile X mental retardation protein and synaptic plasticity. Mol. Brain *6*, 15.

Silverman, J.L., Yang, M., Lord, C., and Crawley, J.N. (2010). Behavioural phenotyping assays for mouse models of autism. Nat. Rev. Neurosci. *11*, 490–502.

Stefely, J.A., and Pagliarini, D.J. (2017). Biochemistry of Mitochondrial Coenzyme Q Biosynthesis. Trends Biochem. Sci. *42*, 824–843.

Strumbos, J.G., Brown, M.R., Kronengold, J., Polley, D.B., and Kaczmarek, L.K. (2010). Fragile X mental retardation protein is required for rapid experience-dependent regulation of the potassium channel Kv3.1b. J. Neurosci. *30*, 10263–10271.

Szabó, I., and Zoratti, M. (1991). The giant channel of the inner mitochondrial membrane is inhibited by cyclosporin A. J. Biol. Chem. *266*, 3376–3379.

Tranfaglia, M.R. (2011). The psychiatric presentation of fragile x: evolution of the diagnosis and treatment of the psychiatric comorbidities of fragile X syndrome. Dev. Neurosci. *33*, 337–348.

Udagawa, T., Farny, N.G., Jakovcevski, M., Kaphzan, H., Alarcon, J.M., Anilkumar, S., Ivshina, M., Hurt, J.A., Nagaoka, K., Nalavadi, V.C., et al. (2013). Genetic and acute CPEB1 depletion ameliorate fragile X pathophysiology. Nat. Med. *19*, 1473–1477.

Um, J.W., Kaufman, A.C., Kostylev, M., Heiss, J.K., Stagi, M., Takahashi, H., Kerrisk, M.E., Vortmeyer, A., Wisniewski, T., Koleske, A.J., et al. (2013). Metabotropic glutamate receptor 5 is a coreceptor for Alzheimer aβ oligomer bound to cellular prion protein. Neuron *79*, 887–902.

Vander Heiden, M.G., Cantley, L.C., and Thompson, C.B. (2009). Understanding the Warburg effect: the metabolic requirements of cell proliferation. Science *324*, 1029–1033.

Vlasov, A.V., Kovalev, K.V., Marx, S.H., Round, E.S., Gushchin, I.Y., Polovinkin, V.A., Tsoy, N.M., Okhrimenko, I.S., Borshchevskiy, V.I., Büldt, G.D., et al. (2019). Unusual features of the c-ring of F_1F_O ATP synthases. Sci. Rep. *9*, 18547.

Warburg, O. (1956). On respiratory impairment in cancer cells. Science *124*, 269–270.

Watson, D.J., Ostroff, L., Cao, G., Parker, P.H., Smith, H., and Harris, K.M. (2016). LTP enhances synaptogenesis in the developing hippocampus. Hippocampus *26*, 560–576.

Weisz, E.D., Towheed, A., Monyak, R.E., Toth, M.S., Wallace, D.C., and Jongens, T.A. (2018). Loss of Drosophila FMRP leads to alterations in energy metabolism and mitochondrial function. Hum. Mol. Genet. *27*, 95–106.

Wijetunge, L.S., Chattarji, S., Wyllie, D.J., and Kind, P.C. (2013). Fragile X syndrome: From targets to treatments. Neuropharmacology *68*, 83–96.

Wise, D.R., DeBerardinis, R.J., Mancuso, A., Sayed, N., Zhang, X.Y., Pfeiffer, H.K., Nissim, I., Daikhin, E., Yudkoff, M., McMahon, S.B., and Thompson, C.B. (2008). Myc regulates a transcriptional program that stimulates mitochondrial glutaminolysis and leads to glutamine addiction. Proc. Natl. Acad. Sci. USA *105*, 18782–18787.

Zhang, Y., Brown, M.R., Hyland, C., Chen, Y., Kronengold, J., Fleming, M.R., Kohn, A.B., Moroz, L.L., and Kaczmarek, L.K. (2012). Regulation of neuronal excitability by interaction of fragile X mental retardation protein with slack potassium channels. J. Neurosci. *32*, 15318–15327.

Zheng, X., Boyer, L., Jin, M., Mertens, J., Kim, Y., Ma, L., Ma, L., Hamm, M., Gage, F.H., and Hunter, T. (2016). Metabolic reprogramming during neuronal differentiation from aerobic glycolysis to neuronal oxidative phosphorylation. eLife *5*, e13374.

Zoghbi, H.Y., and Bear, M.F. (2012). Synaptic dysfunction in neurodevelopmental disorders associated with autism and intellectual disabilities. Cold Spring Harb. Perspect. Biol. *4*, a009886.

Please cite this article in press as: Licznerski et al., ATP Synthase c-Subunit Leak Causes Aberrant Cellular Metabolism in Fragile X Syndrome, Cell (2020), https://doi.org/10.1016/j.cell.2020.07.008

STAR★METHODS

KEY RESOURCES TABLE

REAGENT or RESOURCE	SOURCE	IDENTIFIER
Antibodies		
Mouse anti-FMRP 7G1-1	Developmental Studies Hybridoma Bank	https://dshb.biology.uiowa.edu/7G1-1; RRID:AB_528251
Rabbit anti-FMRP	Cell Signaling	Cat. #4317; RRID: AB_1903978
Rabbit anti-Bcl-xL (54H6)	Cell Signaling	Cat. #2764; RRID:AB_2228008
Mouse anti-Puromycin [3RH11]	Kerafast	Cat. #Equation 0001; RRID:AB_2620162
Mouse anti-GAPDH (6C5)	Santa Cruz Biotech.	Cat. #sc-32233; RRID:AB_627679
Rabbit anti-PSD-95	Cell Signaling	Cat. #2507; RRID:AB_561221
Rabbit anti-p-EF2 (Thr56)	Cell Signaling	Cat.#2331; RRID:AB_10015204
Mouse anti-EF2 (F-9)	Santa Cruz Biotech.	Cat. #sc-166409; RRID:AB_2262106
Rabbit anti-ATP5G1/G2/G3 [EPR13908]	abcam	Cat. #ab180149
Mouse anti-ATPB [3D5]	abcam	Cat. #ab14730; RRID:AB_301438
Rabbit anti-COX IV	Cell Signaling	Cat. #4844; RRID:AB_2085427
Mouse anti-Beta-actin [C4]	Santa Cruz Biotech.	Cat. #sc-47778; RRID:AB_626632
Glycolysis Antibody Sampler Kit	Cell Signaling	Cat. #8337; RRID:AB_10897509
Chicken anti-GFP	abcam	Cat. #ab13970; RRID:AB_300798-
Anti-mouse IgG HRP-linked	Cell Signaling	Cat. #7076; RRID:AB_330924
Anti-rabbit IgG HRP-linked	Cell Signaling	Cat. #7074; RRID:AB_2099233
ChromPure mouse IgG, whole molecule	Jackson ImmunoResearch	Cat. #015-000-003; RRID:AB_2337188
ChromPure rabbit IgG, whole molecule	Jackson ImmunoResearch	Cat. #011-000-003; RRID: AB_2337118
Bacterial and Virus Strains		
One Shot TOP10 chemically competent *Escherichia coli*	Invitrogen	Cat. #C404010
Chemicals, Peptides, and Recombinant Proteins		
ABT-737	Selleck Chemicals	Cat. #S1002
Dexpramipexole Dihydrochloride	Sigma-Aldrich	Cat. #SML0392
ACMA (9-amino-6-chloro-2-methoxyacridine)	Sigma-Aldrich	Cat. #A5806
TMRM tetramethylrhodamine, methyl ester	Invitrogen	Cat. #T668
Puromycin Dihydrochloride from *Streptomyces alboniger*	Sigma-Aldrich	Cat. #P8833
D-serine	Sigma-Aldrich	Cat. #S4250
Cyclosporin A	Cell Signaling	Cat. #9973
Lipofectamine 3000 transfection reagent	Thermo Fisher	Cat. #L3000001
Lipofectamine 2000 transfection reagent	Thermo Fisher	Cat. #11668030
EZview Red Anti-FLAG M2 affinity gel	Millipore Sigma	Cat. #F2426
Protein G agarose	Roche	Cat. #11719416001
Protein A/G PLUS agarose	Santa Cruz Biotech.	Cat. #sc-2003
cOmplete, Mini, EDTA-free Protease Inhibitor Cocktail	Roche	Cat. #11836170001
Protector RNase inhibitor	Roche	Cat. #3335399001
RIPA buffer (10x)	Cell Signaling	Cat. #9806
Recombinant Flag-tagged Bcl-xL	This paper	N/A
Critical Commercial Assays		
ATPlite Luminescence Assay System	PerkinElmer	Cat. #6016943
iScript cDNA Synthesis Kit	Bio-Rad	Cat. #1708890

(*Continued on next page*)

Please cite this article in press as: Licznerski et al., ATP Synthase c-Subunit Leak Causes Aberrant Cellular Metabolism in Fragile X Syndrome, Cell (2020), https://doi.org/10.1016/j.cell.2020.07.008

Continued

REAGENT or RESOURCE	SOURCE	IDENTIFIER
TaqMan Gene expression Assays: mouse ATP5G1	Thermo Fisher	Probe ID: Mm02601566_g1
TaqMan Gene expression Assays: mouse ATP5G2	Thermo Fisher	Probe ID: Mm00848143_g1
TaqMan Gene expression Assays: mouse ATP5G3	Thermo Fisher	Probe ID: Mm01334541_g1
TaqMan Gene expression Assays: mouse ATP5B	Thermo Fisher	Probe ID: Mm01160389_g1
TaqMan Gene expression Assays: mouse ActB	Thermo Fisher	Probe ID: Mm02619580_g1
L-lactate Assay Kit I	Eton Bioscience	Cat. #120001 100A
Qproteome Mitochondria Isolation Kit	QIAGEN	Cat. #37612
RNeasy Plus Mini Kit	QIAGEN	Cat. #74134
Deposited Data		
LC/MS/MS full dataset	This Paper	Table S1
Experimental Models: Cell Lines		
Human Embryonic Kidney HEK293	Millipore Sigma	Cat. #12022001
Human WT fibroblast lines sc-173 and sc-176	Dr. Gary J. Bassell	https://www.cores.emory.edu/escc/about/who%20we%20are/gary.html
Human FX fibroblast lines CH095 and sc-128	Dr. Gary J. Bassell	https://www.cores.emory.edu/escc/about/who%20we%20are/gary.html
Human FX fibroblast lines S001, S002, S005	Dr. Elizabeth Berry-Kravis	https://www.rushu.rush.edu/research/departmental-research/pediatrics-research/laboratory-elizabeth-berry-kravis-md-phd
Experimental Models: Organisms/Strains		
Mouse: FVB.129P2-*Pde6b*$^{+}$*Tyr*$^{c\text{-}ch}$/*AntJ*	The Jackson Laboratory	Stock #004828
Mouse: Fmr1$^{-/y}$ (FVB.129P2-*Fmr1*^{tm1Cgr}/*J*	The Jackson Laboratory	Stock #004624
Oligonucleotides		
Please refer to Table S2.	N/A	N/A
Recombinant DNA		
Plasmid: FRET based ATP reporter ATeam YEMK	Imamura et al., 2009	N/A
Plasmid: c-subunit expression	Alavian et al., 2014	N/A
Plasmid: Bcl-xL expression	Li et al., 2013	N/A
Plasmid: Dendra translation indicator	Dr. Deanna Benson	https://icahn.mssm.edu/profiles/deanna-l-benson
Software and Algorithms		
Prism 8.0.0 (131)	GraphPad Software, Inc.	https://www.graphpad.com
ImageJ	NIH	https://imagej.nih.gov/ij/
Scaffold4 proteome software	Proteome Software Inc.	http://www.proteomesoftware.com/products/scaffold/

RESOURCE AVAILABILITY

Lead Contact

Further information and requests for resources and reagents should be directed to and will be fulfilled by the Lead Contact, Elizabeth A. Jonas (elizabeth.jonas@yale.edu).

Materials Availability

All unique/stable reagents generated in this study are available from the Lead Contact without restriction. For reagents please contact Elizabeth A. Jonas (lead contact) (elizabeth.jonas@yale.edu).

Please cite this article in press as: Licznerski et al., ATP Synthase c-Subunit Leak Causes Aberrant Cellular Metabolism in Fragile X Syndrome, Cell (2020), https://doi.org/10.1016/j.cell.2020.07.008

Data and Code Availability

The published article includes all datasets generated or analyzed during this study. Original data for the LC/MS/MS dataset are included in this manuscript in Table S1. LC/MS/MS source files are available from Pawel Licznerski (pawel.licznerski@yale.edu) on request without restrictions.

EXPERIMENTAL MODEL AND SUBJECT DETAILS

Mice

Wild-type (WT) (FVB.129P2-*Pde6b*$^{+}$*Tyr*$^{c\text{-}ch}$/*Ant*) and Fmr1$^{-/y}$ (FVB.129P2-*Fmr1*^{tm1Cgr}/*J*) mice were purchased from Jackson Laboratories (Bar Harbor, MA). All procedures were performed in accordance with the NIH Guidelines for the Care and Use of Laboratory Animals and approved by Yale University's Institutional Animal Care and Use Committee (IACUC).

Human fibroblast lines

Human FX and WT cell lines were kindly shared by Dr. Gary J. Bassell laboratory (Emory University, Atlanta, GA) and Dr. Elizabeth Berry-Kravis (Rush University Medical Center, Chicago, IL).

Cells were cultured in high glucose DMEM supplemented with 10% v/v FBS, 100 U/ml penicillin, 100 μg/ml streptomycin (all from GIBCO).

METHOD DETAILS

Mice hippocampal primary cultures

Primary hippocampal neurons were prepared from mouse embryos (WT or FX male and female pups at E19), as described previously (Beaudoin et al., 2012; Kaech and Banker, 2006; Li et al., 2008). Briefly, after isolation of hippocampi from prenatal brains, neurons were dissociated and plated (0.15×10^6 cells/ 35mm plate) in plating medium with 5% FBS. After 2-4 hr incubation, plating medium was changed to neurobasal medium supplemented with B-27, glutamine, and antibiotics (Invitrogen GIBCO life technologies, Carlsbad, CA). Neurons were grown at 37°C in a 5% CO_2 and 20% O_2 humidified incubator.

Mouse cortical primary cultures

Cortical cultures were prepared from P0-P2 FVB (WT control) and FMRP KO pups as described in Beaudoin et al. (2012).

Dendra translation indicator

Plasmid coding for Dendra embedded in the 5′ and 3′ UTR of beta-actin was kindly shared by Dr. Deanna Benson (Icahn School of Medicine at Mount Sinai, New York, NY). Cells were transfected using Lipofectamine 2000 (Invitrogen) and experiments were performed at DIV14-21. When Dendra is translated *in vitro*, it emits green fluorescent light. Green fluorescence is photoconverted to red fluorescence by exposure to fluorescent light 400-490 nm for 2 min., after which the newly developing green fluorescence represents newly translated actin reporter. Measurements were obtained at 5 min. after photoconversion, using a Zeiss Axiovert 200 microscope and analyzed for fluorescence intensity (center of the soma) using ImageJ software.

ABT-737 treatment

A stock solution of ABT-737 (Selleckchem, Houston, TX) was prepared in dimethyl sulfoxide (DMSO). ABT-737 (1 μM) or the same volume of DMSO was added into the culture dishes for mRNA translation studies.

Cyclosporine A

Cyclosporine A (CsA) was purchased from Cell Signaling and stock solution was prepared in dimethyl sulfoxide (DMSO). Primary neuronal cortical cultures at DIV 14-16 were treated with 0.2 to 0.5 μM CsA (final concentration) or DMSO as a control for 6 hours, harvested, lysed and processed for further analysis.

Dexpramipexole

A dose of Dex for *in vivo* treatment was chosen by searching the literature and analyzing previous reports on Dex metabolism (Bozik et al., 2011; Cudkowicz et al., 2011; Muzzi et al., 2018). A stock solution of Dexpramipexole dihydrochloride (SIGMA-ALDRICH, St. Louis, MO) was prepared in sterile dH_2O and used at different concentrations described in the manuscript.

DNA plasmid transfections

All neuronal cultures were transfected at day 5-7 DIV (days *in vitro*) using Lipofectamine 2000 reagent (Invitrogen), according to the manufacturer's specifications. The same reagent was used to transfect human fibroblast lines. Vector for c-subunit expression was the same as previously used and described by Alavian et al. (2014).

siRNA

DsiRNA (Integrated DNA Technologies, USA) stocks were prepared according to the manufacturer's protocol. Transfections of siRNA (final concentration: 25 pmol per well) were performed using Lipofectamine 2000 reagent (Invitrogen). Cell lysates were prepared 20-24 hours post transfection.

Control DsiRNA:

Sense: CGUUAAUCGCGUAUAAUACGCGUAT
Antisense: AUACGCGUAUUAUACGCGAUUAACGAC
c-subunit DsiRNA (hs.Ri.ATP5G1.13.1):
Sense: CCAGUGAAUUCAUCUAAACAGCCTT
Antisense: CGGGUCACUUAAGUAGAUUUGUCGGAA

Purification of recombinant Bcl-xL

Flag-tagged Bcl-xL (Li et al., 2013) was immunoprecipitated from HEK293T cell lysates using the EZview Red ANTI-FLAG M2 Affinity Gel (Sigma-Aldrich) according to the manufacturer's protocol. The purified protein samples were examined by western blot.

Puromycin incorporation for measurement of protein synthesis

Puromycin (Puromycin dihydrochloride, SIGMA-ALDRICH) labeling was performed as previously described (Schmidt et al., 2009). Briefly, cells or synaptosomes were incubated in puromycin containing media (10 μg/ml) for 15 minutes, washed twice with cold PBS, lysed in 1xRIPA buffer (Cell Signaling) containing proteinase inhibitors (Roche, Indianapolis, Indiana) and phosphatase inhibitors PhosSTOP (Roche Diagnostics GmbH, Mannheim, Germany).

For *in vivo* studies adult (2 month or older) mice were injected (IP) with (30 mg/kg) puromycin (SIGMA ALDRICH). After 2.5 hr animals were sacrificed and brain and liver samples were harvested and homogenized in 1xRIPA buffer (Cell Signaling) containing proteinase inhibitors (Roche, Indianapolis, Indiana) and phosphatase inhibitors PhosSTOP (Roche Diagnostics GmbH, Mannheim, Germany) and processed for western blot analysis. Alternatively, adult mice were sacrificed and 200 μm brain slices containing prefrontal cortex were incubated in hippocampal recording buffer (with 95% O_2 and 5% CO_2) containing (in nmol): 125 mM NaCl, 25 mM $NaHCO_3$, 2.5 mM KCl, 25 mM glucose, 1.25 mM NaH_2PO_4, 1 mM $MgCl_2$, 2 mM $CaCl_2$ bubbled with 95%O_2, 5% CO_2, for 2.5 hr. with Dexpramipexole (final concentration 10 μM). For the last 15 minutes of incubation puromycin was added to the bath (final 10 μg/ml). Next, brain slices were homogenized in 1xRIPA buffer (Cell Signaling) containing proteinase inhibitors (Roche, Indianapolis, Indiana) and phosphatase inhibitors PhosSTOP (Roche Diagnostics GmbH, Mannheim, Germany) and processed for western blot analysis.

Immunoprecipitation of puromycin labeled peptides

Isolated synaptosomes or P0-P2 FVB or FX DIV14-16 cortical cultures were treated for 15 min. with puromycin. 50-100 μg of protein from cell lysate, was incubated at 4°C overnight with 1 μg of anti-puromycin antibody (Kerafast). Next, 50 μL of protein G agarose (Roche Diagnostics GmbH) was added to samples for an overnight incubation at 4°C. Beads were washed 3 times with 1x RIPA buffer (Cell Signaling) and processed for mass spectrometry analysis. For experiments with Dexpramipexole, cortical cultures were treated with 10 μM Dex for 2-24 hours prior to puromycin treatment and then processed for western blot.

Co-immunoprecipitation of FMRP and the beta- and c-subunit of the ATP synthase

WT and FX purified synaptosomal lysates were incubated at 4°C overnight with 10 μg of mouse anti-FMRP 7G1-1 (developed by Stephen T. Warren, this antibody was obtained from the Developmental Studies Hybridoma Bank developed under the auspices of NICHD and maintained by the University of Iowa, Department of Biological Sciences, Iowa City IA 55242) or 10 μg of mouse IgG. Next, immunoprecipitates were immobilized on A/G agarose beads (Santa-Cruz Biotechnology) at 4°C overnight and washed 4-5x15 minutes with 1x RIPA lysis buffer (Cell Signaling) with 40 U/ml protector RNase inhibitor (Roche) and 1x Complete EDTA-free protease inhibitor cocktail tablet (Roche). mRNA was purified from beads using the quickRNA purification kit (QIAGEN) according to the manufacturer's protocol. RNAs were then reverse transcribed using a cDNA reverse transcription kit (Biorad) according to the manual. Next, a standard PCR reaction was run using the following primers:

GGCAAGATGGGGTATAGAGA; Map1b forward primer
CCCACCTGCTTTGGTCTTTG; Map1b reverse primer
AAGCTGGAGAACAACTTGGAC; Arc forward primer
CCCCCAAGACTGATATTGCTGAG, Arc reverse primer

Primer sequences above have been published by Brown et al. (2010).

GCCAGAGACTATGCGGCGCAG; mATP5B forward primer
GGACCTCTCTCATCAATAGG; mATP5B reverse primer

GGCCTGTGTCTGCCTCCCTCC; mATP5G1 forward primer
GGCGACCATCAAACAGAAGAG; mATP5G1 reverse primer
GAGCACCTCTCAGCTGCTGAGTCG; mATP5G2 forward primer
GGCCTCTGAGAGGGCAAAGCC; mATP5G2 reverse primer
GTTCGCCTGCGCCAAGCTCGC; mATP5G3 forward primer
GTGAAGGGTTTCAGCACCAG; mATP5G3 reverse primer

Western blot analysis

Brain tissue or primary neuronal culture lysates or mitochondrial lysates were prepared using RIPA lysis buffer (Cell Signaling) containing proteinase inhibitors (Roche, Indianapolis, Indiana) and phosphatase inhibitors PhosSTOP (Roche Diagnostics GmbH, Mannheim, Germany). The protein concentration was measured using a BCA kit (Pierce, Rockford, Illinois). Then, protein samples were electrophoretically separated on an SDS-PAGE gel (4%–20% gradient gel, Bio-Rad, USA) and transferred overnight to PVDF membranes (0.2 μm pores, Bio-Rad, USA). The membranes were incubated in 2% BSA (Tris-buffered saline (TBS), 0.1% Tween 20) for 1 h and then incubated at 4°C overnight with primary anti-Bcl-xL (1:1000, Cell Signaling), anti-puromycin (1:1000, Kerafast), anti-GAPDH (1:1000, Santa Cruz Biotechnology), anti-PSD-95 (1:1000, Cell Signaling), anti-p-EF2 (1:1000, Cell Signaling), anti-EF2 (1:1000, Santa Cruz Biotechnology), anti-ATP5g1/2/3 (1:1000, abcam), anti-ATPb (1:1000, abcam), anti-beta-actin (1:1000, Cell Signaling), anti-FMRP (1:1000, Cell Signaling). Antibodies for glycolytic enzyme detection were supplied by Glycolysis Antibody Sampler Kit #8337, Cell Signaling and used at 1:1000 dilution. After 3 × 15 min washes membranes were incubated for 1 h with secondary, horseradish peroxidase (HRP) conjugated antibodies (1:5000, Cell Signaling) and developed using a chemilluminescence kit (Pierce, Rockford, Illinois).

Blue Native Page Electrophoresis

Protein complexes from 20 μg (verified by BCA assay) of mitochondria (per lane) were separated on Bis-Tris 3%–12% Native gels. Samples were solubilized on ice for 20 minutes with 4 μg digitonin/μg protein. After separation the protein complexes were wet-transferred onto a polyvinylidene fluoride (PVDF) membrane, which was probed with anti-ATP5G1,2,3 antibody for ATP synthase c-subunit.

Isolation of mitochondria

Mitochondria were isolated and purified from mouse brain as previously described (Ofengeim et al., 2012; Sacchetti et al., 2013). In brief, brain tissue was homogenized in isolation buffer (250mM sucrose, 20mM HEPES, 1mM EDTA, 0.5% BSA). After a series of centrifugations, the nuclear material, cytosolic fraction and the mitochondrial pellet containing synaptosomes were separated. Synaptosomes were disrupted by applying 1200 psi pressure for 10min and mitochondria were separated by ultracentrifugation (Brown et al., 2004) . To isolate mitochondria from human fibroblasts, a Qproteome^{TM} Mitochondria isolation kit was used (QIAGEN, Cat.37612), according to the manufacturer's protocol.

Isolation of SMVs from mouse brain

FVB or FMRP KO mouse brain tissue (without cerebellum) was homogenized in ice-cold isolation buffer (250 mM sucrose, 20 mM HEPES (pH 7.2), 1 mM EDTA, and 0.5% BSA). After a brief centrifugation at 1,500 g, the supernatants were centrifuged at high-speed (16,000 × g) for 10 min at 4°C. The crude pellets were re-suspended in isolation buffer and a pressure of 1,200psi was applied for 10min, followed by rapid decompression. The pure mitochondrial fraction was then pelleted in a ficoll density gradient by centrifugation and washed with isolation buffer. Non-ionic detergents (digitonin and Lubrol-PX) were used to further solubilize and stabilize membrane-bound protein complexes, and the sub mitochondrial vesicles (SMVs) were isolated by a final 2 hr ultracentrifugation (Chan et al., 1970; Sacchetti et al., 2013). Freshly prepared SMV protein amount was quantified using the Bradford protein assay

Preparation of synaptosomal fractions

Synaptosomal fractions were prepared as previously described (Alavian et al., 2011). Briefly, cultured neurons were homogenized in isotonic mitochondrial buffer and centrifuged at 600 x g for 10 min at 4 °C. The pellet, containing the nuclear and unbroken cells, was discarded and the supernatant, containing the mitochondrial, synaptosomal and cytosolic fractions, was centrifuged at 10,000 g for 30 min at 4 °C. The supernatant, containing the cytosolic fraction, was separated from the pellet. The pellet containing the mitochondrial and synaptosomal fractions was resuspended in 100 μL isolation buffer and layered onto a 7.5%–10% Ficoll gradient. After 30 min ultracentrifugation at 90,000 g, 4 °C, the mitochondrial pellet and the middle layer, containing synaptoneurosomes (hereafter called synaptosomes) were removed. The synaptosomal layer was resuspended in isolation buffer and centrifuged for 10 min at 20,000 g, resulting in a crude synaptosomal pellet.

D-serine stimulation of synaptosomes

Synaptosomal samples purified from FVB and FMRP KO mice and were stimulated with D-serine (final concentration 0.2 μM), supplied in extracellular (EC) recording buffer without magnesium (120mM NaCl, 4mM KCl, 2mM $CaCl_2$, 10mM HEPES, 10mM

D-Glucose, pH = 7.4). 1 μg of puromycin was also added to measure protein synthesis. EC buffer lacking D-serine was added to unstimulated control samples. Samples were harvested and lysed in 1xRIPA at 3, 5, 15 and 30 minutes post stimulation.

Quantitative Real Time RT-PCR

Total RNA was extracted from FVB and FX synaptosomes using RNeasy Plus Mini Kit according to the manufacturer's protocol (QIAGEN). Next, extracted RNA was reverse transcribed using Bio-Rad iScript first cDNA synthesis kit. TaqMan® Gene Expression Assays (Thermo Fisher Scientific, USA) was used to quantify mRNA levels. Data were analyzed using the $2^{-\Delta\Delta CT}$ method using beta-actin as the normalizing endogenous control. The following probes were used: mATP5G1 (Mm02601566_g1), mATP5G2 (Mm00848143_g1), mATP5G3 (Mm01334541_g1), mATP5B (Mm01160389_g1), mActB (Mm02619580_g1).

Measurement of ATP levels in Figure 1

Primary cortical neurons were seeded onto 96 well plates (0.015×10^6 neurons/ well). After 1-2 weeks incubation, cells were treated as stated in relevant figure legends. ATP production was measured by using ATPlite™ Luminescence Assay System (PerkinElmer, Waltham, MA) according to the manufacturer's protocol. Cells were washed with sterile PBS, lysed and incubated with substrate (luciferin) for 15 min. The reaction between ATP, luciferase and luciferin produced bioluminescence. ATP-induced-luminescence was measured with a VICTOR^3 multilabel reader (PerkinElmer, Waltham, MA).

Measurement of mitochondrial potential ($\Delta\psi$)

Mitochondrial membrane potential ($\Delta\psi$) was measured using the fluorescent lipophilic cationic dye tetramethylrhodamine methyl ester (TMRM, Invitrogen, Molecular Probes, Carlsbad, CA, USA), which accumulates within mitochondria in a membrane potential-dependent manner. Primary hippocampal neurons were stained with 5 nM TMRM for 30 min at 37°C in the dark. Images were taken using a Zeiss LSM 710 confocal scanning microscope and TMRM fluorescence densitometry was analyzed using ZEN software (Carl Zeiss Microscopy GmbH, Jena, Germany).

ACMA assay

ACMA (9-amino-6-chloro-2-methoxyacridine, Sigma A5806) fluorescence quenching was measured as previously described (Alavian et al., 2011) with some modifications. In brief, 2μM ACMA and 50 μg of the isolated mouse brain submitochondrial vesicles (SMVs), were used. SMV suspension fluorescence was measured at 490 nm using a PerkinElmer VICTOR3 (PerkinElmer, Waltham, MA) multilabel plate reader.

Lactate assay

Growth media were collected at DIV20 from WT and FX neuronal primary cultures treated with either 5 μM Dex or vehicle daily from DIV15 to DIV20. Lactate levels in the growth medium samples were calculated using the L-Lactate assay Kit I (Eton Bioscience, Charlestown, MA) according to the manual provided.

SMV ion channel recordings

SMV recordings were made by forming giga-ohm seals onto SMVs in intracellular solution (120 mM KCl, 8 mM NaCl, 0.5 mM EGTA, 10 mM, HEPES (pH 7.3)) using an Axopatch 200B amplifier (Axon Instruments) at room temperature (22–25°C). Recording electrodes were pulled from borosilicate glass capillaries (WPI) with a final resistance in the range of 50–120 MΩ. Signals were filtered at 5 kHz using the amplifier circuitry. Data were analyzed using pClamp 10.0 software (Axon Instruments). Membrane currents under different experimental conditions were assessed by measuring peak membrane current (in pA). All current measurements were adjusted for the holding voltage assuming a linear current-voltage relationship: The resulting conductances are expressed in pS according to the equation G = I/V where G is conductance in pS, V is the membrane holding voltage in mV, and I is the peak membrane current in pA. Group data were quantified in terms of conductance. All population data were expressed as mean ± SEM.

Brain Electron microscopy

Brain slices from FVB (WT) and FMRP KO adult mice (over 2 month-old) were incubated in artificial cerebral spinal fluid (ACSF) containing (in mM): 125 mM NaCl, 25 mM $NaHCO_3$, 2.5 mM KCl, 25 mM glucose, 1.25 mM NaH_2PO_4, 1 mM $MgCl_2$, 2 mM $CaCl_2$ bubbled with 95%O_2, 5% CO_2 with vehicle or 0.2 μM Cyclosporin A for 2 hr 45 min. Samples were fixed in 4% paraformaldehyde in 0.25M HEPES for 1 hour. Samples were rinsed in PBS and re-suspended in 10% gelatin, chilled and trimmed to smaller blocks and placed in cryoprotectant of 2.3M sucrose overnight on a rotor at 4°C. They were transferred to aluminum pins and frozen rapidly in liquid nitrogen. The frozen block was trimmed on a Leica Cryo-EMUC6 UltraCut and 65-75nm thick sections were collected using the Tokoyasu method. The frozen sections were collected on a drop of sucrose, thawed and placed on a nickel formvar/carbon coated grid and floated in a dish of PBS ready for immunolabeling. Grids were placed section side down on drops of 0.1M ammonium chloride to quench untreated aldehyde groups, then blocked for nonspecific binding on 1% fish skin gelatin in PBS. All grids were rinsed in PBS, fixed using 1% glutaraldehyde for 5mins, rinsed and transferred to a UA/methylcellulose drop, then dried for viewing. Samples were viewed FEI Tencai Biotwin TEM at 80Kv. Images were taken using Morada CCD and iTEM (Olympus) software. Analysis of electron micrographs was performed using ImageJ software (NIH).

Please cite this article in press as: Licznerski et al., ATP Synthase c-Subunit Leak Causes Aberrant Cellular Metabolism in Fragile X Syndrome, Cell (2020), https://doi.org/10.1016/j.cell.2020.07.008

Dendritic spine density analysis and ATP measurement

Hippocampal neurons were isolated from E18.5-19 FMRP KO and WT mice using enzymatic digestion with Trypsin EDTA (GIBCO) followed by mechanical trituration and then cultured in Neurobasal media with 1 X B27 supplement (GIBCO). Half of the medium was replaced with fresh medium every week. Cells were transfected at DIV1 with the ATeam ATP reporter construct (Imamura et al., 2009) (kindly provided by Dr. Imamura and Dr. Noji from Osaka University, Osaka, Japan) using Lipofectamine 3000 (Thermo Fisher) as per manufacturer's recommendations. Cells were treated with 5 μm Dexpramipexole additively for 6 consecutive days from DIV 15 – DIV 20. At DIV 20 conditioned medium was collected for measurement of lactate levels.

For quantification of dendritic spines, cells were fixed at DIV 20 with 4% buffered formalin and immuno-stained with anti-GFP antibody (Abcam, ab13970). Images were acquired with a Zeiss 880 Airyscan microscope. Dendritic spines were accessed visually on the basis on their morphology; mature spines were identified by their mushroom-like shape; all other spines were considered immature (see illustration in Figure 6).

ATP levels were measured in neurons at DIV 20 using the well characterized FRET based ATP reporter ATeam YEMK (Imamura et al., 2009a) in a HEPES (10 mM) based buffer containing NaCl (125 mM), KCl (3 mM), $CaCl_2$ (2 mM), $MgCl_2$ (2 mM) and D-Glucose (5 mM). For LTP stimulation of neurons, 10 μM D-Serine was applied in the same buffer but lacking $MgCl_2$ for 5 min. FRET measurements were performed with a Zeiss 710 confocal microscope equipped with a controlled atmosphere cabinet at 25°C. Measurements of changes in pH using a pH sensitive indicator were performed separately and did not show any significant changes in pH before or after stimulation during the times of acquisition of ATP signal.

Mass Spectrometry

Following separation of protein complexes in one-dimension by SDS-PAGE, protein bands of interest were excised for bottom-up protein identification by LC/MS/MS. Gel bands were prepared as described (Glass et al., 2017). Briefly, excised gel bands in 1.5 Eppendorf tubes are washed 4 times; first with 500 μL 60% acetonitrile containing 0.1%TFA and then with 5% acetic acid, then with 250 μL 50% H_2O/50% acetonitrile followed by a 250 μL 50% CH_3CN/ 50 mM NH_4HCO_3, and a final wash with 250 μL 50% CH_3CN/10 mM NH_4HCO_3 prior to removal of wash and complete drying of gel pieces in a Speed Vac. 10 μL of a 0.1 mg/mL stock solution of trypsin (Promega Trypsin Gold MS grade) in 5mM acetic acid is freshly diluted into a 140 μL solution of 10mM NH_4HCO_3 to make the working digestion solution. 124 μL of the working digestion solution is added to the dried gels pieces (additional 10 mM NH_4HCO_3 was added to ensure gel pieces are completely submerged in the digestion solution) and incubated at 37°C overnight. Sample is then stored at −20°C until analysis. Tryptic peptides were separated on a nanoAcquity UPLC column (Waters) coupled to a Q-Exactive Plus mass spectrometer. High resolution tandem LC MS/MS data were collected by Higher-Energy Collisional Dissociation (HCD) with a 1.4 Da window followed by normalized collision energy of 32%. Resulting LC MS/MS data were analyzed and processed through Proteome Discoverer (v.2.2 and linked to MASCOT search engine v.2.4) and further integrated with Scaffold (v.4.8, Proteome Software Inc.).

Behavioral experiments

Male FVB (WT) and $Fmr1^{-/y}$ mice 2 months of age were used for all experiments. All animal procedures were in accordance with US National Institutes of Health standards and approved by the Yale University Institutional Animal Care and Use Committee. Prior to behavioral testing mice were handled individually by the investigator to decrease anxiety. Next, mice received 3 IP injections of Dex (10 mg/kg) over the course of 40 hours: two injections separated by 24 hour period and the third 16 hours after the second injection. Behavioral testing started 2-3 hours after the last (third) injection. For repetitive behaviors (grooming and nestlet shredding) (Angoa-Pérez et al., 2013; Silverman et al., 2010) mice were placed in a new, empty home cage and their behavior was monitored during 10 minute sessions, video recorded and scored manually. Grooming was identified as body licking or stroking, scratching of the head or body with the two forelimbs. Attempts at grooming were defined as a total number of grooming events during the 10 minute session. For nestlet shredding mice were placed in a new empty home cage without bedding with one cotton nestlet and recorded for 10 minutes. Nestlet shreds were collected and weighed. Exploratory locomotion (total time moving, walking plus running) was assessed during a 5 minute session, recorded and scored manually (Baker et al., 2010; Dolan et al., 2013). The investigator was blinded as to the genetic variant during scoring.

QUANTIFICATION AND STATISTICAL ANALYSIS

Statistical analysis was performed using Prism 8 (GraphPad Software, San Diego, CA). Data are presented as mean ± SEM. Paired or unpaired Student's two-tailed t test was used for two group comparisons. For multiple comparisons, one-way or two-way ANOVA test with Tukey post hoc test was used. Statistical details and methods used in each experiment can be found in figures and in the figure legends. $p < 0.05$ is considered statistically significant. *p* values are provided in figure legends (*$p < 0.05$; **$p < 0.01$; ***$p < 0.001$; ****$p < 0.0001$).

Supplemental Figures

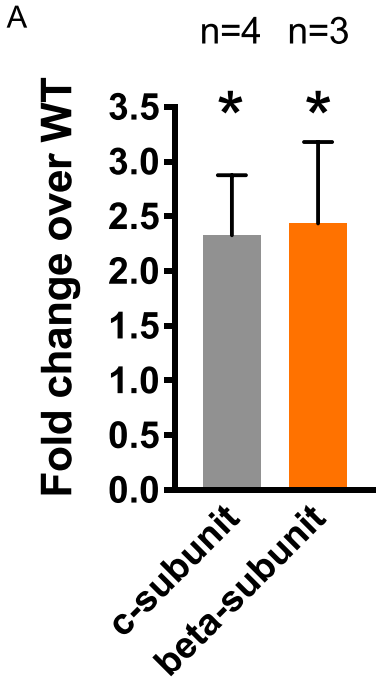

Figure S1. qRT-PCR Expression Profile of c-Subunit (ATP5G2) and β-Subunit mRNA from Synaptosomes, Related to Figures 2 and 5

Shown is fold change of *Fmr1*$^{-/y}$ over WT (n = 4 and 3 different animals, *p < 0.05). Unpaired two-tailed Student's t test was used. Data are represented as mean ± SEM (*p < 0.05; **p < 0.01; ***p < 0.001; ****p < 0.0001)

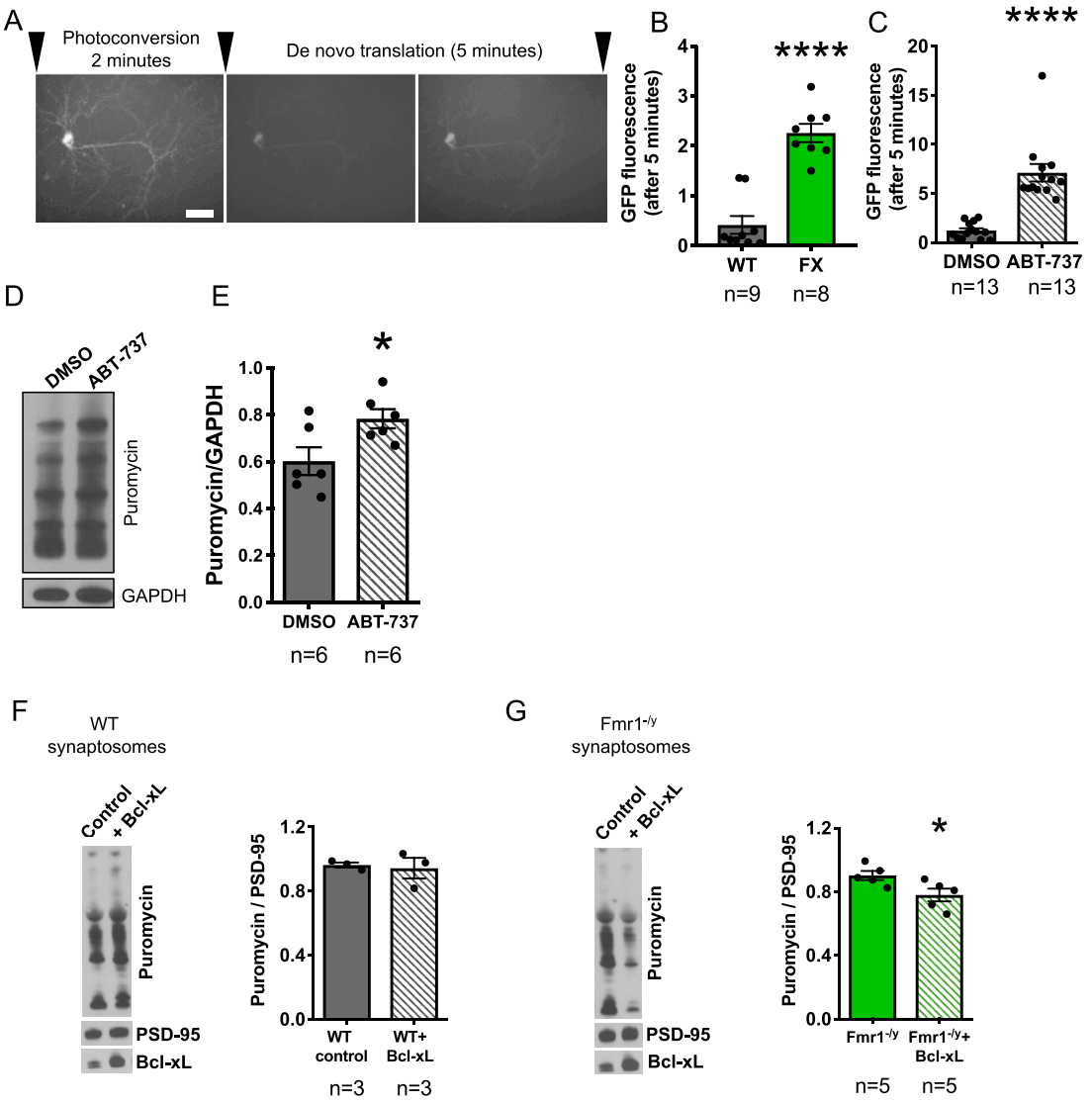

Figure S2. Protein Synthesis Rate Is Elevated in FX Neurons, Related to Figure 4

(A) Representative images of Dendra in isolated cortical neurons before, just after, and 5 minutes after photoconversion (see methods). (B) The rate of translation of Dendra during 5 min after photoconversion in WT and FX mouse neurons. (C) The rate of translation of Dendra in WT neurons exposed to vehicle (DMSO) or 1 μM Bcl-xL inhibitor, ABT-737 for 20 min. (D, E) Puromycin incorporation over 15 minutes in WT cortical neurons exposed to 1 μM ABT-737 or vehicle control (DMSO) for 1 hour prior to puromycin application. (F, G) Example of puromycin assay before and after transfection of recombinant Bcl-xL protein (0.045-0.79 mg/ml) into synaptosomes. Bcl-xL represses protein translation in FX but not in WT. (F) Group data for puromycin incorporation for WT control samples. (G) Group data for puromycin incorporation for FX samples from at least three different animals (*p = 0.037). Unpaired two-tailed Student's t test. Data are represented as mean ± SEM (*p < 0.05; **p < 0.01; ***p < 0.001; ****p < 0.0001)